1 **Introduction**

2 **Stream Water Composition: Arsenic, Uranium, and Stable Water Isotopes**

3 **Characterizing Arsenic and Uranium Contamination through Isotopic and Hydrologic Inference**

4 **Conclusion**

Stable water isotopes provide insight into the spatial variability of As and U in drinking water across the Northern Plains

Jacob Abbott

Winter 2023

Abstract

Arsenic (As) and uranium (U) contamination in drinking water affects millions of individuals across the US. This issue is particularly acute across rural populations where many people obtain drinking water from unregulated private wells. One specific location greatly affected by high levels of As and U in both surface and groundwater is the Northern Plains of the USA. However, the environmental and anthropogenic factors responsible for the mobilization and heterogeneous distribution of As and U in the waters of this region remain poorly characterized. Groundwater recharge sources and the flow path of water supplying surface water can strongly influence the mobilization and accumulation of aqueous As and U. To understand how hydrologic process affect the distribution of these metals we relied on stable water isotopes (δ^2H, $\delta^{18}O$, $\delta^{17}O$). Here we collected stream and spring water samples from 43 locations across South Dakota and Nebraska and measured stable water isotopes (δ^2H, $\delta^{18}O$, $\delta^{17}O$) to determine the sources of recharge/inflow to both surface water and groundwater (e.g., heavily evaporated surface water, snow melt, precipitation). We observe strong positive correlations between As and U and stable water isotopes – a finding that suggests that mobilization of these elements is occurring under oxic conditions, mobilization is delocalized, and As and U are likely accumulating along the water's flow path. These results allow for a greater understanding of how hydrology influences As and U occurrence in surface water and groundwater and can be used to help better predict areas at high risk for As and U contamination.

1 Introduction

The water cycle is one of the most recognizable and understandable environmental phenomena on the earth. It controls much of the world we know today and is fundamental in the long-term geomorphology of the planet. Furthermore, access to water from this cycle is necessary for human survival. Across the globe, numerous methods are used for collecting, storing, and moving this natural resource. One of the most prominent of these processes is the collection and manipulation of groundwater. Worldwide, over 2 billion people rely on groundwater for their everyday needs (Hackley 2018). This includes 115 million people in the United States which is approximately ⅓ of the current population (Communications and Publishing 2015). This widespread use has resulted in the depletion of our natural groundwater sources (Konikow and Kendy 2005). Furthermore, this overuse has caused the deterioration of water quality, damage to local ecosystems, and irreversible land subsidence (Konikow and Kendy 2005). Another issue is that many wells are unregulated. Approximately, 43 million Americans use private wells which do not fall under the regulation of the Federal Safe Drinking Water Act or state laws (Resources 2019b). This means the safety of their water is the responsibility of the homeowner which often is not economically feasible.

Despite the importance of many groundwater aquifers and other drinking water sources, many contain harmful contaminants including chemicals, metals, and pathogens. Some common contaminants include Giardia, E. Coli, Lead, Salmonella, and Arsenic (*Water Contamination and Diseases* 2022). The World Health Organization (WHO) estimates that 1 in 3 people don't have access to safe drinking water (*1 in 3 People Globally Do Not Have Access to Safe Drinking Water – UNICEF, WHO* 2019). This is a major issue as poor water quality accounts for around 1.7 million deaths annually (Ashbolt 2004). A majority of these deaths occur in children and are primarily in developing countries (Ashbolt 2004). Additionally, exposure to metals such as arsenic has been linked to neurodevelopmental issues (Bondy and Campbell 2017). Mothers in Bangladesh were at higher risk for giving birth to infants with neural defects when exposed to high arsenic levels (Bondy and Campbell 2017). Another threat to global freshwater sources is climate change. One main effect of climate change is an increase in floods and droughts. This has had effects on water availability and has affected water quality and safety (Delpla et al. 2009). Land evolution events such as deforestation and urban spreading heavily affect water quality (Delpla et al. 2009). These issues combined with rising temperatures and higher pollution load define why water is listed as one of the UN's global issues (*Global Issues*, n.d.).

Two metals or metalloids (referred to hereafter as metals) associated commonly with poor drinking water are arsenic(As) and uranium(U). Arsenic and uranium can be found in almost any lithological setting. Some areas with studied high arsenic levels include Argentina, Chile, Mexico, China, Hungary, India, Bangladesh, and Vietnam (Smedley and Kinniburgh 2002). While these countries have shown elevated levels of the metal, arsenic can still be found elsewhere including in drinking water across all 50 states (*Arsenic* 2021). In trace amounts, arsenic and uranium are both seen as safe to consume. The EPA sets guideline values of 10 µg/L and 30 µg/L for arsenic and uranium respectively but it is best to avoid any contamination if possible (*Chemical Contaminant Rules* 2022). This is not the easiest task as according to WHO, over 140 million people have been drinking water containing arsenic at levels above the guideline value (*Arsenic* 2022). It was also found that 2.1 percent of US communities reported average uranium water concentrations above the EPA guideline (Ravalli et al. 2022). The issue with consuming these metals is they have been associated with a host of negative health conditions. For arsenic, this includes skin cancer, cardiovascular diseases, and diabetes (WHO, 2022). For uranium, this includes hypertension, cardiovascular disease, kidney damage, and lung cancer (Ravalli et al. 2022). The Centers for Disease Control and Prevention (CDC) estimated 38.4% of US deaths in 2020 were caused by cancer and cardiovascular diseases alone making it a major concern (*Leading Causes of Death* 2023).

The primary route of exposure to arsenic and uranium is through the consumption of contaminated groundwater (*Arsenic Factsheet* 2017; *What Are the Routes of Exposure for Uranium?* 2013). Groundwater is found within aquifers which are defined as a body of permeable rock that is capable of storing and transporting groundwater. Within these aquifers, contaminants can accumulate through natural and anthropogenic processes. One trait of both arsenic and uranium is that they do not originate in groundwater. Rather, these metals naturally occur in rock and sediment and can be mobilized when in the presence of water under particular geochemical conditions. The mobilization of arsenic can happen under either oxidizing or reducing conditions, however, in most cases of geogenic arsenic contamination, arsenic is mobilized under reducing conditions in most environments (Herath et al. 2016). Once reducing conditions are met, the mobilization of absorbed arsenic from amorphous Fe(iron) oxides, which are abundant in aquifer sediments, can occur (Herath et al. 2016). Uranium typically is mobilized through processes such as mineral dissolution and desorption of absorbed uranium (Alam and Cheng 2014). The most notable difference between these two minerals is that arsenic favors release in reducing conditions and uranium favors release in oxidizing conditions which implies that both metals should, in general, not be present in the same locations. Exceptions to this include mineral

dissolution and mining (Smedley and Kinniburgh 2002). Mineral dissolution occurs in mineralized areas where redox conditions mobilize arsenic into groundwater (Smedley and Kinniburgh 2002). Mining can also accelerate the mobilization of arsenic and uranium by exposing minerals to weathering conditions (*The Role of Arsenic in the Mining Industry* 2015). Once arsenic and uranium are released into an aquifer, groundwater flow takes over moving the now-contaminated water until it is discharged to the surface or pulled out by a well.

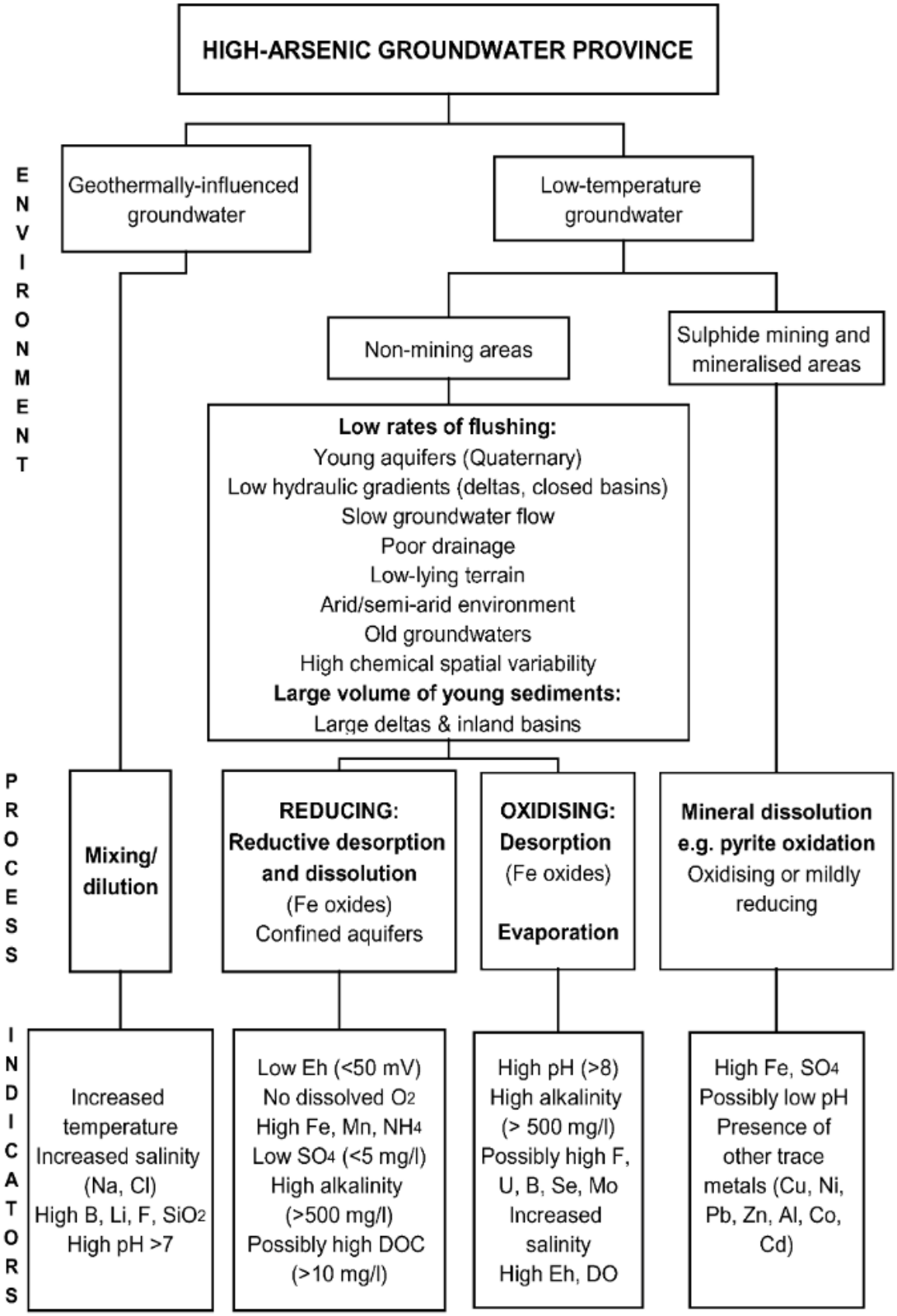

Figure 1.1: Arsenic mobilization pathways from Smedley and Kinniburgh (2002).

One of the main causes of this widespread exposure to contamination is the use of unregulated wells. The USGS estimated that over 2.1 million people in the US might be drinking well water with high Arsenic values (Resources 2019c). Many of these people live in rural areas of the country making it challenging to identify these hazardous wells (Shaw, Walker, and Benson 2005). Furthermore, arsenic is naturally occurring and contamination is often not due to human impacts making it hard to spatially map without proper research. Another crucial element is groundwater arsenic contamination is not limited to low-population areas. As seen in Bangladesh, a South Asian country with over 165 million people, arsenic levels in groundwater wells are way above the WHO guideline (Fendorf, Michael, and Geen 2010). In this region, elevated levels of arsenic were seen to be caused by elevated pumping of groundwater which altered the natural regional flow pattern (Fendorf, Michael, and Geen 2010). This elevated pumping lowered the water table causing arsenic-rich sediment deposited in rivers to be flushed out into the local aquifers (Fendorf, Michael, and Geen 2010). Another way exposure to arsenic can occur is through the consumption of metal-rich crops. While direct consumption of contaminated water is the primary cause of arsenic ingestion, irrigation can enhance arsenic uptake into plants (Azizur Rahman et al. 2008). One of the most impacted plants is rice which has been found to be a major potential source of arsenic exposure (Mondal and Polya 2008). Unfortunately, one commonality between these examples and many others is that arsenic contamination disproportionately affects members of socio-economically disadvantaged communities (Balazs et al. 2012).

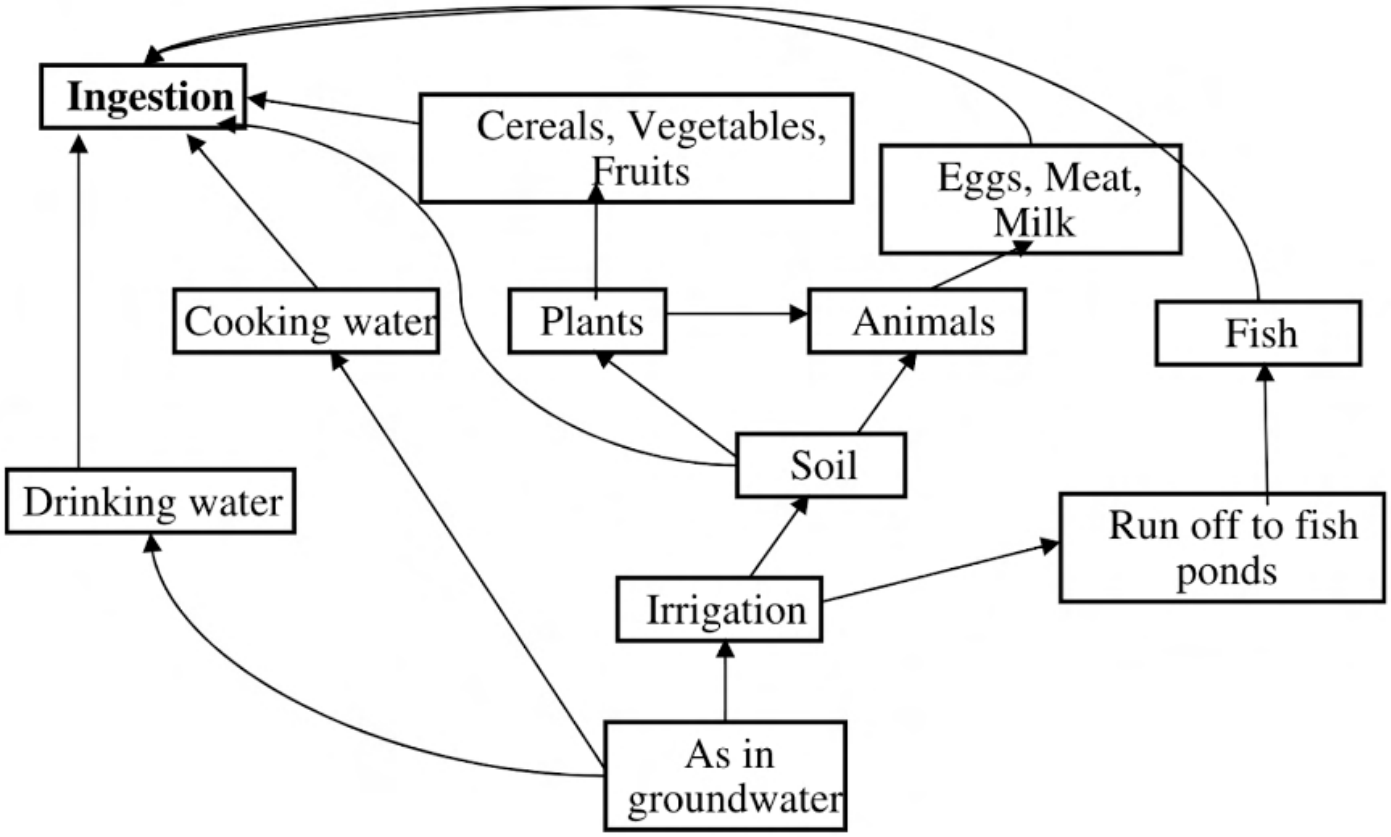

Figure 1.2: Arsenic consumption pathways from Mondal and Polya (2008).

One group of people commonly affected by contaminated water are indigenous American people, specifically the Ogallala Lakota tribes located in the Pine Ridge Reservation, SD. Positioned at the bottom of South Dakota and at the top of the High Plains aquifer, this reservation spans 3,468.85 sq mi (8,984 km2) making it one of the largest in the country. The most notable nearby features in the region include the Badlands National Park, The White River, and Mount Rushmore but despite this, they are one of the poorest counties in the nation (Medzerian, Newman, and O'Connell 2022). The population of the people living on the reservation is 19,157, consisting primarily of indigenous Ogallala tribe members (*American Community Survey 5-Year Estimates* 2021). Many of the people in this community are put at high risk for contamination from water quality impairments.

As a result of poor regulations on private groundwater wells, these individuals have been exposed heavily to arsenic and uranium. The long-running Strong Heart Study (SHS) performed on the reservation has documented high urinary arsenic and uranium levels in tribal study sites relative to the general US population (Sobel et al. 2021). Much of this exposure likely comes from drinking groundwater with elevated levels of metals but other sources such as contaminated food and excessive smoking could further elevate contamination levels (*Arsenic Factsheet* 2017). It was found that indigenous American smoking rates in adults and youth were the highest in the nation (Geishirt Cantrell et al. 2005). Despite these reasons, there is some community unrest concerning where the metal contamination is coming from, specifically local mines (Personal Communication). One such mine is Crow Butte an in-situ uranium mine located near the reservation (Leonard 2021). While it is possible that contaminants were released through the in-situ recovery process, preliminary evidence suggests that this mine is not a source of contamination.

One way to determine the source of contamination is by analyzing the stable water isotopes δD, $\delta^{18}O$, and $\delta^{17}O$. Stable isotopes are non-radioactive forms of atoms that often naturally occur in nature (*Stable Isotopes*, n.d.). The δ values of water can be found by proportionately comparing lighter isotopes to their heavy counterparts in this case $^{18}O/^{16}O$ and $^{2}H/^{1}H$ ($\delta^{2}H$ is also known as δD) . We can use these isotopes as tracers to fully understand the in and outflow of groundwater as well as determine water origin and any other environmental effects such as evaporation. Crucially, groundwater, surface water, and precipitation all have unique isotopic values allowing for easy differentiation. Another important factor is that precipitation isotopes when compared against groundwater isotopes, allow us to determine the groundwater recharge source(s) and the seasonal timing of this recharge which can help us better understand local aquifers (M. O. Stahl, Gehring, and Jameel 2020). By linking the source(s) and timing of groundwater recharge to measured groundwater arsenic levels we can better identify the hydrologic and geochemical processes that control the observed variability in groundwater arsenic levels (Nghiem et al. 2019). These factors are important in helping to determine local arsenic contamination sources and the environmental drivers of arsenic mobilization.

The primary aim of this study is to leverage the spatial data to understand the mobilization mechanisms of As and U into drinking water in the Northern Plains. We hypothesize that (1) redox disequilibrium drives the spatial variations in As and U levels, and thereby influences exposure, (2) isotopes can be used to determine mobilization models, and (3) surface features may strongly predict the occurrence of groundwater arsenic and uranium.

This thesis is part of a larger 5-year project through Columbia University and is structured as follows. Chapter 2 will focus on the spatial relationships between arsenic and uranium compared to isotopes. In Chapter 3, we will implement end-member mixing models to determine the water sources and flow direction in the study area. Chapter 4 will summarize key findings and outline future research.

2 **Stream Water Composition: Arsenic, Uranium, and Stable Water Isotopes**

2.1 **Introduction**

To understand the spatial distribution of arsenic and uranium spatially quantify groundwater in the Pine Ridge Reservation groundwater, I will be using surface water to compare and contrast arsenic, uranium, and stable water isotopes. The interconnection between surface water and groundwater plays a crucial role in understanding the exchange between these two systems (Kalbus, Reinstorf, and Schirmer 2006). Across South Dakota, there are numerous geological formations of notability. The first is the large surficial deposits of glacial till spanning half of the state (Martin et al. 2004). These deposits are located entirely on the eastern side of the state and are largely outside of our study area (Martin et al. 2004). Next, is the Black Hills located just northwest of the Pine Ridge Reservation. This formation was formed 70 million years ago when Precambrian granite uplifted through sedimentary rock (*Geologic Activity* 2020). This sedimentary rock then began to weather leaving behind the resistant granite (*Geologic Activity* 2020). The eroded material was then transported downstream where it formed the next notable formation, the Badlands (*Geologic Activity* 2020). The Badlands National Park (Figure 2.1) is located across the northwest corner of the Pine Ridge reservation and is the primary geological formation in the region. It is made up of layers containing sandstones, siltstones, mudstones, claystones, limestones, volcanic ash, and shale (*Geologic Formations: How Badlands Buttes Came to Be* 2020). These have since been eroded leaving deep valleys across the region.

Figure 2.1: Badlands National Park taken by Jacob Abbott on 13-AUG-2022.

An impactful feature in the Pine Ridge Reservation is the White River. This river is a Missouri tributary that flows 580 miles through South Dakota and Nebraska (*National App*, n.d.). It gets its name from the white color of the sediment in its water which is picked up as it passes through the Badlands. It has a drainage basin of approximately 10,200 square miles and an average discharge of 618 cubic feet per second between 1929 and 2021 (6446500, n.d.). The largest storms tend to fall during the summer months (Figure 2.2) but the majority of recharge is predicted to come from winter precipitation. This is backed up by the hydrograph showing the increase in water height during the winter months and early spring while there is a general decrease despite frequent storms in the summer months (Figure 2.2). Oglala Lakota County, the main county in the reservation, gets around 17.3 inches of precipitation per year which is lower than the 2020 national average of 30.3 inches (*Oglala Lakota County, South Dakota Precipitation*, n.d.; *Monthly National Climate Report for Annual 2020* 2021). Due to its central location, this precipitation comes from both local vapor sources and from vapor sources as far away as the oceans.

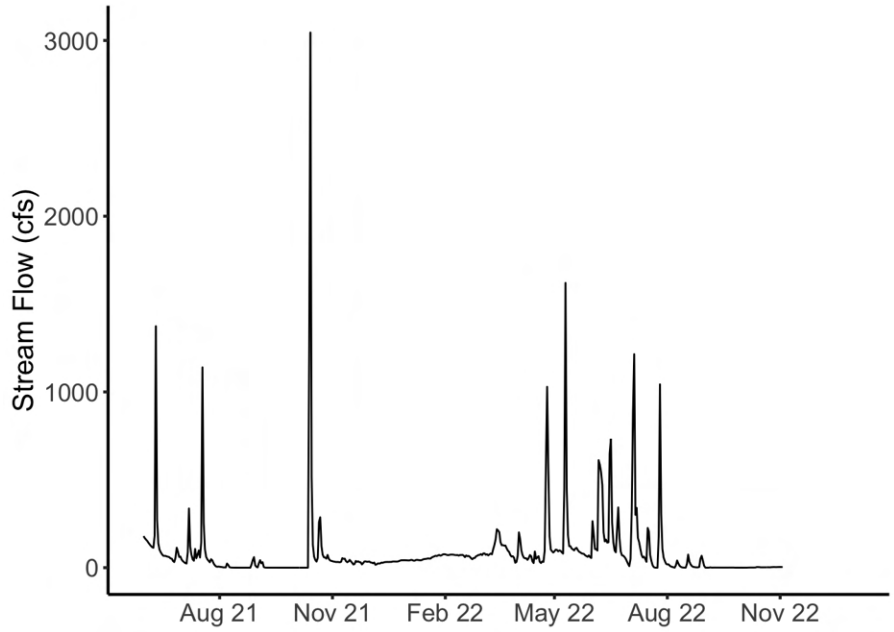

Figure 2.2: 2021-2022 Hydrograph from USGS monitoring location 06446500 at the White River in Jackson County

The geology of the Pine Ridge Reservation is broken up into four main geologic layers (Figure. **X**). The upper layer is Quaternary Eolian deposits of silt and sand with depths of up to 300 ft (Martin et al. 2004). Located just below this layer are the Ogallala group formations, which consist primarily of sandstone (Martin et al. 2004). The first of the main two formations is the Arikaree group. This group contains the Rosebud, Harrison, Turtle Butte, Monroe Creek, and Sharps formations (Martin et al. 2004). They have thicknesses between 65ft to 360ft and contain variations of siltstone, sandstone, claystone, and volcanic ash (Martin et al. 2004). The primary aquifer layer is the White River group which consists of the Brule, Chadron, Chamberlain Pass, and Slim Buttes formations (Martin et al. 2004). This formation has thicknesses from 32ft to 160 ft and similarly to the Arikaree group contains variations of siltstone, sandstone, claystone as well as bentonite and mudstone (Martin et al. 2004). These aquifers are all underlain by a confining layer of clay and silt ("Ground Water Atlas of the United States: Segment 8, Montana, North Dakota, South Dakota, Wyoming" 1996). Flow through these aquifers generally follows topography toward the White River and its tributaries (Carter and Heakin 2007).

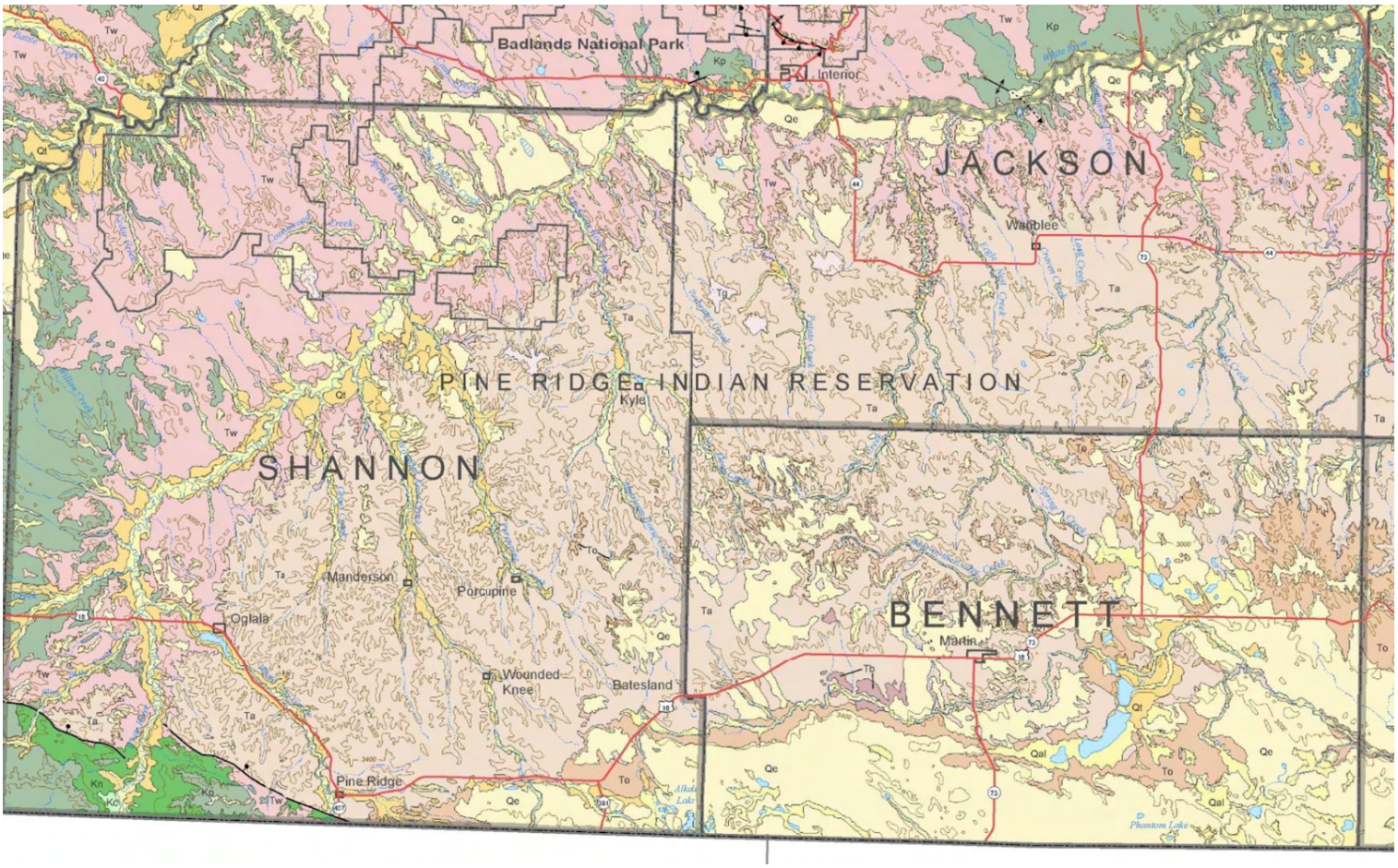

Figure 2.3: Pine Ridge Reservation geologic formations from the Martin et al. (2004). Qe is Quaternary Eolian deposits, To is Ogallala group formations, Ta is Arikaree group formations, and Tw is White River group formations.

2.2 **Methods**

Field methods

For my study 43 surface water samples were collected with 10 collected in August 2022, 22 collected in July 2021, and 12 collected in December 2021. Samples were collected from various locations across the Pine Ridge Reservation region and were primarily located where streams and roads intersected. Using a 60ml syringe, water was collected and then filtered into a 15ml centrifuge tube using a 0.2-micron polyethersulfone (PES) syringe filter. Some samples were left unfiltered in the field due to the abundance of suspended micro-particles. Coordinates, site information, and pictures were also collected at each location. Samples collected for stable water isotope analysis were refrigerated prior to analysis. Samples collected for ICP-MS analysis were acidified with trace metal grade nitric acid (to pH < 2) and refrigerated prior to analysis.

Lab methods

Prior to analysis, samples that were not previously filtered were filtered again with a 0.2-micron PES syringe filter and then were transferred into 2 mL glass vials. The few samples that were unable to be filtered were spun in a centrifuge to unsuspend sediment and were then filtered. Filtered vials were analyzed using Union College's Picarro L2140-i coupled with a high-precision A0211 vaporizer and an A0325 autosampler to collect δD, $\delta^{18}O$, and $\delta^{17}O$ isotopes. The Picarro L2140-i was run in ^{17}O mode using ultra-high purity air as the carrier gas. Each sample (vial) was measured on 15 injections with the first 10 injections discarded to help minimize carrier over between samples. Isotopic reference waters SLAP, SMOW, USGS-47, USGS-48, and USGS-49 were analyzed at the start of each run as well as after every 15-20 samples. Isotopic reference standards were run in a sequence SLAP, USGS-47, USGS-48, then SMOW with three vials of each standard used in the sequence. After two cycles three vials of USGS-49 were sampled last. USGS-47 and USGS-48 were used as the calibration standards. Note that SLAP was not used on samples with the title "ND" but the sequence remained the same with SLAP removed (Table 2). The data from each run was calibrated using the known standards. The calibration calculations were performed using an R script. Water was analyzed at Columbia University with an ICP-MS to collect the water chemistry of 34 different elements. The dissolved concentrations of relevant trace elements were measured via an Element 2 inductively coupled plasma mass spectrometer using germanium as an internal standard to correct for instrument drift (Geen et al. 2013; Sun et al. 2016). Data cleaning and combination were completed with the joint use of R and Excel. Further figures and writing was also created in R.

Map & Table

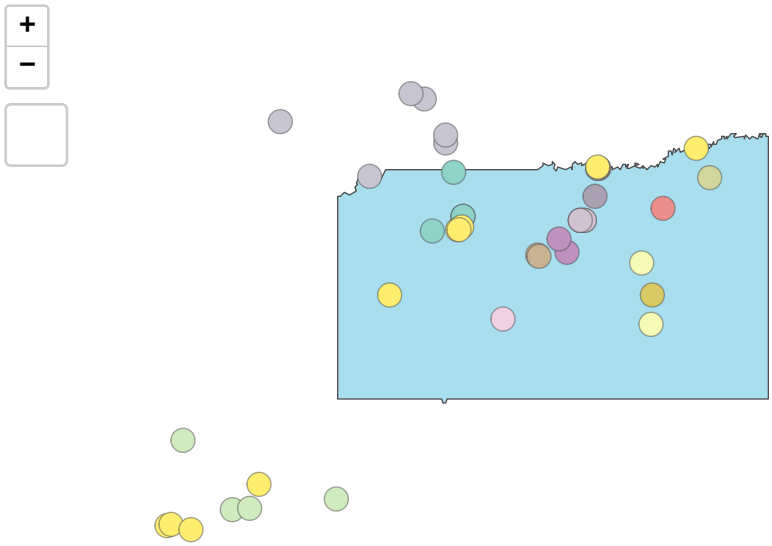

Figure 2.4: Location of points within the study area. Pine Ridge Reservation can be seen as the large blue box. Colors indicate groupings found in Table 1.

Table 2.1: Sample Location Groups

Region	Location	Latitude	Longitude	Date
White River	WR1	43.31353	-102.7885	2022-08-13
	WR3	43.50829	-102.5054	2022-08-13
	WR5	43.69342	-101.9294	2022-08-13
	ND_WR1	42.61936	-103.7045	2021-07-01
	ND_WR2	42.62004	-103.6900	2021-07-01
	ND_WR3	42.60742	-103.6083	2021-07-01
	ND_WR4	42.74484	-103.3260	2021-07-01
	ND_WRB1	43.69371	-101.9334	2021-07-01
	ND_WRB10	43.75207	-101.5249	2021-07-01
	ND_WRB2	43.51471	-102.4925	2021-07-01
	BB06	43.50807	-102.5049	2021-12-01

Region	Location	Latitude	Longitude	Date
Upper White River Basin	ND_CBR1	42.66618	-103.4373	2021-07-01
	ND_CBR2	42.66977	-103.3639	2021-07-01
	ND_CCR	42.69875	-103.0077	2021-07-01
	ND_WC1	42.87641	-103.6407	2021-07-01
Bad Lands	CC1	43.54801	-102.4877	2022-08-13
	ND_CC1	43.54783	-102.4874	2021-07-01
	BB07	43.50511	-102.6096	2021-12-01
	BB08	43.67937	-102.5219	2021-12-01
Lost Dog Creek	LD1	43.69134	-101.9271	2022-08-13
	ND_PC4	43.69039	-101.9322	2021-07-01
	BB01	43.60680	-101.9421	2021-12-01
Medicine Root Reservoir	MR1	43.43186	-102.1790	2022-08-13
	BB05	43.42935	-102.1733	2021-12-01
Porcupine Creek	ND_PCQ1	43.24137	-102.3188	2021-07-01
Redwater Creek	ND_PC1	43.43989	-102.0555	2021-07-01
	BB04	43.48280	-102.0881	2021-12-01
Potato Creek	PC1	43.53578	-101.9861	2022-08-13
	ND_PC2	43.53528	-102.0003	2021-07-01
	ND_PC3	43.53465	-102.0009	2021-07-01
	BB02	43.53581	-101.9859	2021-12-01
	BB03	43.53534	-102.0043	2021-12-01
Bear-in-the-Lodge Creek	ND_BC1	43.22320	-101.7116	2021-07-01
	ND_BC2	43.41092	-101.7519	2021-07-01
Craven Creek	ND_CVC1	43.57250	-101.6620	2021-07-01
Pass Creek	ND_PAC1	43.66539	-101.4701	2021-07-01
Cheyenne River Basin	CY1	43.66706	-102.8704	2022-08-13
	BC1	43.82897	-103.2397	2022-08-13
	BB09	43.76639	-102.5556	2021-12-01
	BB10	43.78903	-102.5560	2021-12-01
	BB11	43.89776	-102.6432	2021-12-01
	BB12	43.91217	-102.7007	2021-12-01
Other	ND_WM1	43.31217	-101.7083	2021-07-01

2.3 **Locations**

This section shows brief details about each site in the study. Sites have been grouped based on region and surrounding geography. Samples starting with BB and SD were collected by Ben Bostick at two separate times. Remaining samples were collected by Jacob Abbott.

White River

Sites: ND_WR1 / ND_WR2 / ND_WR3 / ND_WR4

Description:

These four sites (ND_WR1, ND_WR2, ND_WR3, and ND_WR4) are located at the headwaters of the White River these samples are positioned in the North-West corner of Nebraska. They are located predominantly n grassy land with some occasional bordering farmland.

WR1

Figure 2.5: Picture of site WR1 taken on 13-AUG-2022 by Michael Abbott.

Description:

This site (WR1) is located on the White River alone on the western side of the Pine Ridge reservation. This was the only sample collected between head water and central points and serves to contrast water quality changes. As seen in the image the water was cloudy but was filtered easily.

ND_WRB2 / BB06 / WR3

Figure 2.6: Picture of site WR3 taken on 13-AUG-2022 by Michael Abbott.

Description:

These sites (NDWRB2, BB06, and WR3) are located on the same bend of the white river near the Badlands National Park. The stream bed is notably dry with little water flowing downstream. The water also has the consistency of chocolate milk and was not filterable. Changes in stream quality between this sample location and the WR1 sample location can be seen. These samples are notably before the confluence of the White River and Cottonwood Creek.

ND_WRB1 / WR5 / ND_WRB10

Figure 2.7: Picture of site WR5 taken on 13-AUG-2022 by Michael Abbott.

Description:

These three sites (ND_WRB1, WR5, and ND_WRB10) are located in the center of the Pine Ridge Reservation's northern border. Water quality is similar to the previous White River samples but the river's channel is much wider and there is more flow.

Upper White River Basin

ND_WC1 / ND_CBR1 / ND_CBR2 / ND_CCR

These sites (ND_WC1, ND_CRB1, ND_CRB2, and ND_CCR) are located around the headwaters of the White River positioned in the North-West corner of Nebraska. They are predominately smaller streams with lower flow.

Bad Lands Region

CC1 / ND_CC1

Figure 2.8: Picture of site CC1 taken on 13-AUG-2022 by Michael Abbott.

Description:

This site (CC1 and ND_CC1) is located on the edge of the Badlands National Park and is one of the larger tributaries coming out of the region. One notable feature of the site is the large erosion barriers protecting a bridge. The water quality was very poor and the samples were not filterable.

BB07 / BB08

Description:

These sites (BB07 and BB08) are located in the central parts of the Badlands National Park (Figure 2.1). They are both part of the BB winter samples and less is know about their sample location details.

Lost Dog Creek

BB01

Description:

This site (BB01) is located upstream of the other Lost Dog Creek sites toward the center of the reservation. It is part of the BB winter samples and less is know about its sample location details.

ND_PC4 / LD1

Figure 2.9: Picture of site LD1 taken on 13-AUG-2022 by Michael Abbott.

Description:

These sites (ND_PC4 and LD1) are located a few hundred meters upstream from the ND_WRB1 / WR5 White River sites. The water had noticeably less sediment than the nearby White River samples but was still un-filterable.

Medicine Root Reservoir

MR1 / BB05

Figure 2.10: Picture of site MR1 taken on 13-AUG-2022 by Michael Abbott.

Description:

This reservoir (MR1 and BB05) is located in the very center of the Pine Ridge Reservation. The water was clear and clean with no signs of sedimentation. The reservoir is held back by a dam leading into Medicine Root Creek.

Porcupine Creek

ND_PCQ1

Description:

This site (ND_PCQ1) is located in Porcupine Creek in the western central section of the Pine Ridge Reservation. It is part of one of the longer tributaries in the region.

Redwater Creek

ND_PC1 / BB04

Description:

These samples (ND_PC1 and BB04) fall on Redwater Creek in the center of the Pine Ridge Reservation.

Potato Creek

PC1 / BB02 / BB03 / ND_PC2 / ND_PC3

Figure 2.11: Picture of site PC1 taken on 13-AUG-2022 by Michael Abbott.

Description:

These samples (PC1, BB02, BB03, ND_PC2, and ND_PC3) are located on 2 nearby sections of Potato Creek, are located near the center of Pine Ridge Reservation. The stream is much smaller than other locations and has lots of noticeable terrestrial and aquatic vegetation.

Bear-in-the-Lodge Creek

ND_BC1 / ND_BC2

Description:

These samples (ND_BC1 and ND_BC2) are located farthest east in the Pine Ridge Reservation and are on one of the longer White River tributaries.

Craven Creek and Pass Creek

ND_CVC1 / ND_PAC1

Description:

These samples (ND_CVC1 and ND_PAC1) are located in the North East corner of the Pine Ridge Reservation and are the farthest downstream tributaries for the White River.

Cheyenne River Basin

CY1

Figure 2.12: Picture of site CY1 taken on 13-AUG-2022 by Michael Abbott.

Description:

This sample (CY1) is on the Cheyenne River located outside the study area between Pine Ridge Reservation and Mount Rushmore. Despite neighboring the White River, the Cheyenne River has much more water and hos minimal sedimentation.

BC1

Figure 2.13: Picture of site BC1 taken on 13-AUG-2022 by Jacob Abbott.

Description:

Battle Creek (BC1) is located far outside the study area at the base of the Black Hills. It serves as a control sample to compare to samples within the White River system.

BB09 / BB10 / BB11 / BB12

Description:

These samples (BB09, BB10, BB11, and BB12) are located farthest North in the study area and are on tributaries to the Cheyenne River. They are both part of the BB winter samples and less is know about their sample location details.

Other Locations

ND_WM1

Description:

This sample (ND_WM1) is located in the South East section of the Pine Ridge Reservation and is a tub of water next to a likely groundwater pumping windmill.

2.4 **Results**

Table 2.2: Sample Location Groups

Location	Date	δD(‰)	δ18O(‰)	δ17O(‰)	Δ17O(per meg)	Arsenic(µg/L)	Uranium(µg/L)	Dexcess
CY1	2022-08-13	-87.341	-9.983	-5.260	23.367	1.220520	11.265000	-7.477

Location	Date	δD(‰)	δ18O(‰)	δ17O(‰)	Δ17O(per meg)	Arsenic(µg/L)	Uranium(µg/L)	Dexcess
PC1	2022-08-13	-113.742	-14.890	-7.871	19.188	11.071680	12.301080	5.378
CC1	2022-08-13	-17.421	0.069	0.017	-19.081	82.813840	46.458800	-17.973
BC1	2022-08-13	-87.822	-11.914	-6.287	21.859	9.245979	2.609171	7.490
LD1	2022-08-13	-29.806	0.347	0.153	-29.726	38.677200	28.086780	-32.582
MR1	2022-08-13	-79.455	-8.664	-4.572	11.819	7.562986	3.311101	-10.143
WR1	2022-08-13	-69.097	-6.110	-3.224	7.384	11.490110	9.089861	-20.217
WR3	2022-08-13	-15.231	1.926	0.982	-34.291	56.756450	43.864340	-30.639
WR5	2022-08-13	-23.557	0.481	0.218	-35.700	68.193620	41.093490	-27.405
ND_BC1	2021-07-01	-110.058	-14.231	-7.522	17.555	10.377650	4.896757	3.790
ND_BC2	2021-07-01	-105.321	-13.329	-7.048	11.374	8.536609	5.036722	1.311
ND_CBR1	2021-07-01	-113.380	-15.053	-7.978	-1.608	3.036608	3.923925	7.044
ND_CBR2	2021-07-01	-112.378	-14.880	-7.864	20.408	3.924991	5.672967	6.662
ND_CC1	2021-07-01	-28.082	-1.885	-1.009	-13.467	45.176680	22.001780	-13.002
ND_CCR	2021-07-01	-110.888	-14.394	-7.612	13.614	7.551520	10.645600	4.264
ND_CVC1	2021-07-01	-107.478	-14.065	-7.445	6.368	5.574549	7.248261	5.042
ND_PAC1	2021-07-01	-93.077	-11.511	-6.095	-0.384	9.730366	9.147527	-0.989
ND_PC1	2021-07-01	-83.290	-9.652	-5.113	-5.706	4.207683	0.155147	-6.074
ND_PC2	2021-07-01	-116.436	-15.361	-8.134	6.811	11.419550	23.206460	6.452
ND_PC3	2021-07-01	-112.918	-14.550	-7.701	8.668	10.821970	18.171250	3.482
ND_PC4	2021-07-01	-81.862	-9.471	-5.018	-5.764	15.949120	12.871620	-6.094
ND_PCQ1	2021-07-01	-110.002	-13.855	-7.303	37.137	4.556893	7.146385	0.838
ND_WC1	2021-07-01	-77.014	-9.784	-5.156	22.110	30.865350	17.820070	1.258
ND_WM1	2021-07-01	-120.189	-16.068	-8.499	17.780	9.389835	3.506099	8.355
ND_WR1	2021-07-01	-116.703	-15.233	-8.026	46.903	2.675883	4.403090	5.161
ND_WR2	2021-07-01	-113.004	-14.681	-7.763	16.244	3.952064	5.287716	4.444
ND_WR3	2021-07-01	-115.235	-14.944	-7.895	23.745	2.603147	4.588096	4.317
ND_WR4	2021-07-01	-109.795	-14.158	-7.478	22.324	5.399254	9.130444	3.469
ND_WRB1	2021-07-01	-71.565	-7.774	-4.096	15.909	20.076770	17.333870	-9.373
ND_WRB10	2021-07-01	-74.973	-7.949	-4.192	13.442	18.953930	17.174350	-11.381
ND_WRB2	2021-07-01	-85.792	-9.545	-5.033	17.779	12.092860	13.013020	-9.432
BB01	2021-12-01	-89.315	-11.541	-6.102	8.411	5.999025	5.565706	3.013
BB02	2021-12-01	-114.882	-15.345	-8.127	5.207	12.547013	22.215756	7.878
BB03	2021-12-01	-115.797	-15.445	-8.187	-2.371	13.455723	20.958169	7.763
BB04	2021-12-01	-69.599	-7.269	-3.861	-16.901	11.473231	4.629525	-11.447
BB05	2021-12-01	-87.577	-10.471	-5.560	-18.070	9.157387	7.669545	-3.809
BB06	2021-12-01	-95.669	-12.304	-6.486	29.649	6.364771	13.420011	2.763
BB07	2021-12-01	-98.938	-13.365	-7.060	19.454	8.595087	4.709632	7.982
BB08	2021-12-01	-66.296	-8.248	-4.377	-13.386	194.672932	35.144018	-0.312
BB09	2021-12-01	-57.752	-7.203	-3.806	3.809	35.904088	20.159527	-0.128
BB10	2021-12-01	-51.966	-6.237	-3.303	-4.928	4.579357	1.538960	-2.070
BB11	2021-12-01	-97.426	-12.504	-6.617	4.717	1.360328	13.000881	2.606
BB12	2021-12-01	-102.051	-13.376	-7.080	4.650	1.851737	3.782120	4.957

2.5 Discussion

Arsenic and Uranium

Contaminant Distribution

Arsenic and uranium contamination levels in our sampled stream varied across the study area. Arsenic had a range from 1.2 µg/L to 194.6 µg/L with a mean of 19.5 µg/L and uranium had a range from 0.16 µg/L to 46.6 µg/L with a mean of 13.3 µg/L. Both of these means are far above the national drinking water averages of 0.2 µg/L for arsenic and 1.2µg/L for uranium ("Toxicological Profile for Uranium" 2002; "Toxicological Profile for Arsenic" 2007). The distribution of these arsenic samples seen in Figure 2.14 shows that a majority of the points fall around the EPA guideline of 10 µg/L with a majority of this grouping being below it. However, the locations that display high arsenic values often display very high values. There are multiple locations with 3x to 20x the 10 µg/L guideline (Table 2.2). This is noteworthy as short-term exposure to arsenic with concentrations of 130 µg/L has been associated with health effects (Division 2021). Uranium similarly has levels that exceed EPA guidelines at many locations across our study area (Figure 2.15). Despite many samples having both arsenic and uranium being below these guidelines any amount of these metals may pose health issues especially when consumed over long periods of time. The EPA has proposed changing the arsenic guidelines to 5 µg/L and was previously taking comments on changing it to 3 µg/L (*Technical Fact Sheet: Proposed Rule for Arsenic in Drinking Water and Clarifications to Compliance and New Source Contaminants Monitoring* 2000). The EPA also states they are working toward a Maximum Contaminant Level Goal (MCLG) of zero (*Technical Fact Sheet: Proposed Rule for Arsenic in Drinking Water and Clarifications to Compliance and New Source Contaminants Monitoring* 2000). Based on the EPA's proposal for arsenic where the MCL was cut in half (10 µg/L to 5 µg/L), it is worthwhile to examine the number of exceedances that would occur if the uranium MCL was similarly cut in half (30 µg/L to 15 µg/L). The red line in Figure 2.14 and 2.15 symbolizes this proposed change. If this change were to be made the distribution of both arsenic and uranium samples above these new guidelines is much higher than before. Excluding near zero concentrations, any amount of these contaminants in the water is hazardous, and with arsenic having 32 out of 43 samples above 5 µg/L and uranium having 14 of 43 samples above 25 µg/L understanding why we observe these contaminants is key.

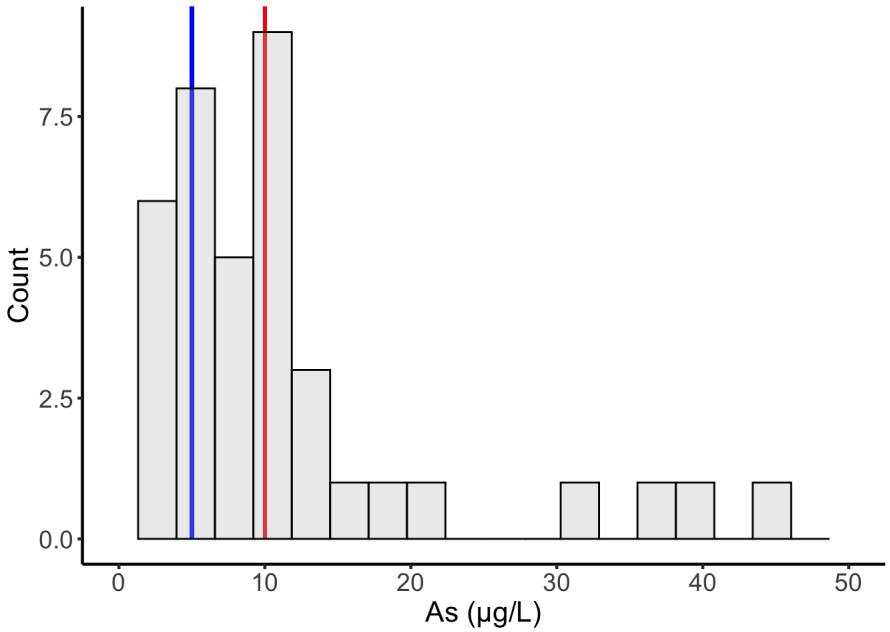

Figure 2.14: Distribution of stream water arsenic concentrations.

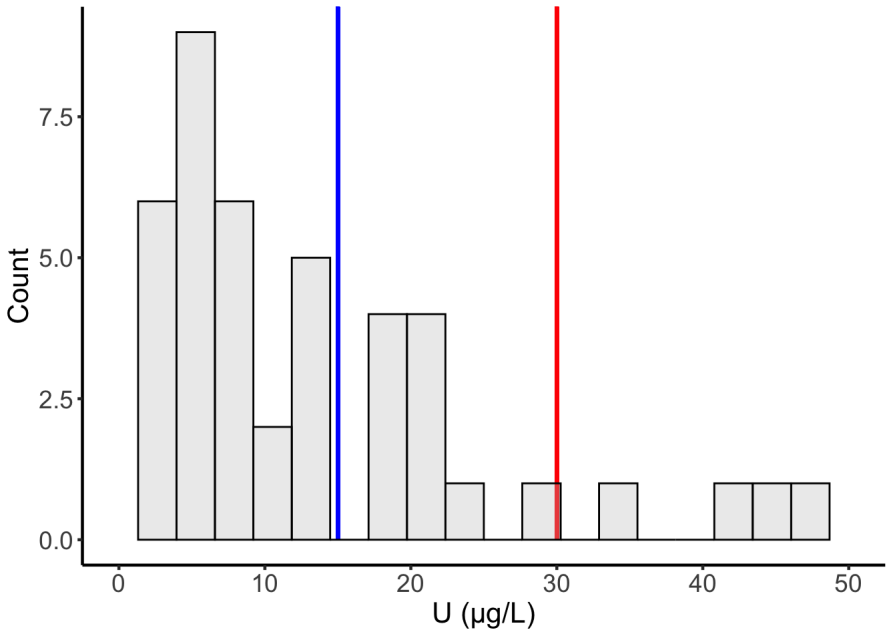

Figure 2.15: Distribution of stream water uranium concentrations.

Mobilization & Concentrations

Arsenic and uranium have numerous different mobilization methods with arsenic often mobilized under reducing conditions (as commonly observed in S-SE Asia) and uranium often mobilized under oxidizing conditions (Fendorf, Michael, and Geen 2010). When these conditions are present one would expect a broadly inverse relationship between aqueous arsenic and uranium concentrations - namely, relatively low arsenic when uranium concentrations are elevated and relatively low uranium when arsenic concentrations are elevated (Yadav et al. 2020). This correlation can be seen in the example Figure 2.16 where uranium-abundant samples (green circle) have low concentrations of arsenic and arsenic-abundant samples (orange circle) have low concentrations of uranium. The primary reason for this is because by definition oxic, containing oxygen, and anoxic, not containing oxygen, can't coexist. This assumption assumes that the conditions present are perfect with no variation which is never truly the case. The lone point in Figure 2.16 (blue circle) breaks this rule as both arsenic and uranium have high concentrations. This inherently implies that a separate mobilization method may have been present resulting in this abnormality.

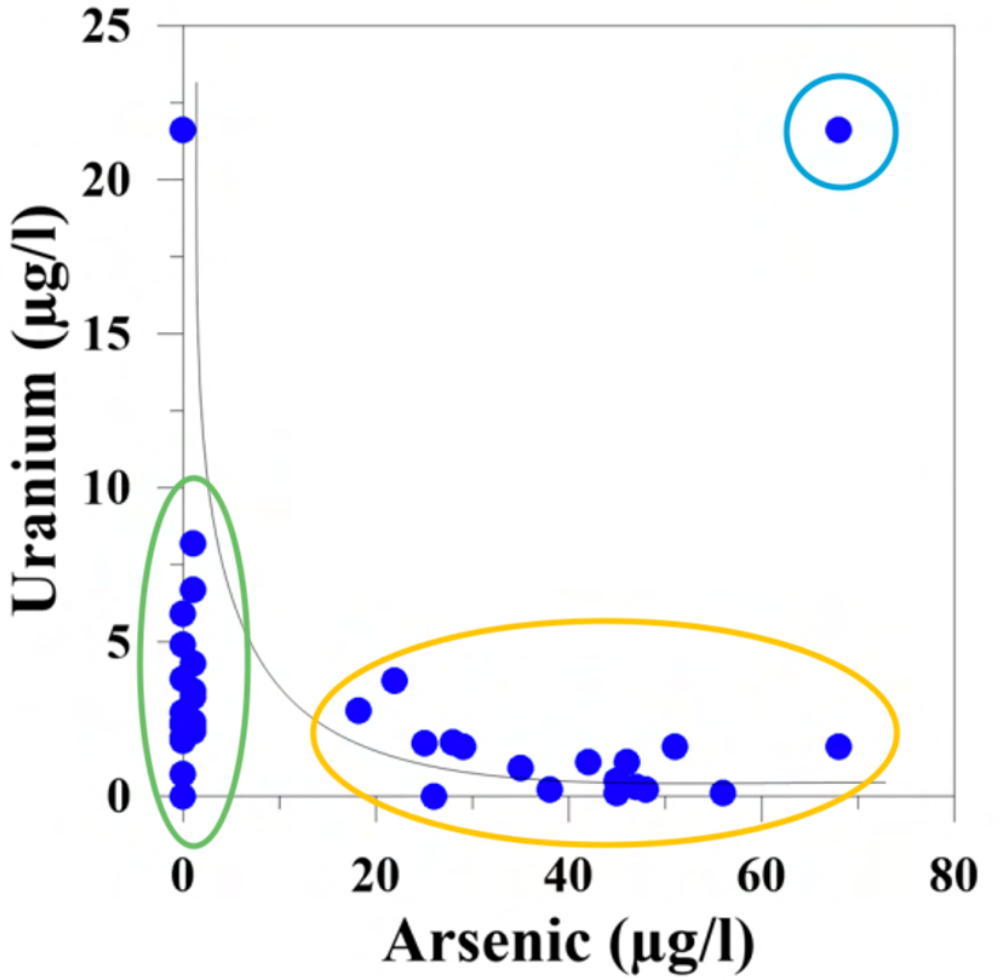

Figure 2.16: Correlation between arsenic and uranium under typical mobilization methods (Figure source: Yadav et al. (2020)). Typically uranium is mobilized under oxic conditons while arsenic is mobilized under reducing conditions. Thus high uranium usualy occurs when arsenic is low (green circle) and high arsenic usualy occurs when uranium is low (orange circle). Blue circle shows outlier. Edited by Jacob Abbott.

Understanding redox conditions (oxic and anoxic) is key for determining possible groundwater contaminants. This includes the previously mentioned arsenic and uranium as well as nitrates and some man-made contaminants (Resources 2019a). One way to predict the likely dominant redox conditions in a aquifer is by using the principal aquifer rock type in conjunction with other environmental factors such as land use and water table depth. Across the US there is a variety of rock types each with their own characteristics (Figure 2.17). Generally, oxic conditions are more prevalent in unconsolidated sand and gravel, basaltic-rock aquifers, crystalline-rock aquifers, and layered sandstone and carbonate aquifers (Resources 2019a). Anoxic conditions in the US are more often in glacial sandstone, carbonate-rock, and semi-consolidated coastal plain aquifers (Resources 2019a). As seen in Figure 2.17, my study area (black box) is located partially within the high plains aquifer (central blue region). This aquifer consists of unconsolidated sand and gravel and primarily has oxic conditions (Resources 2019a). Using this information it can be assumed that the data found in my study area would follow the trends in Figure 2.17 and also primarily be uranium dominant.

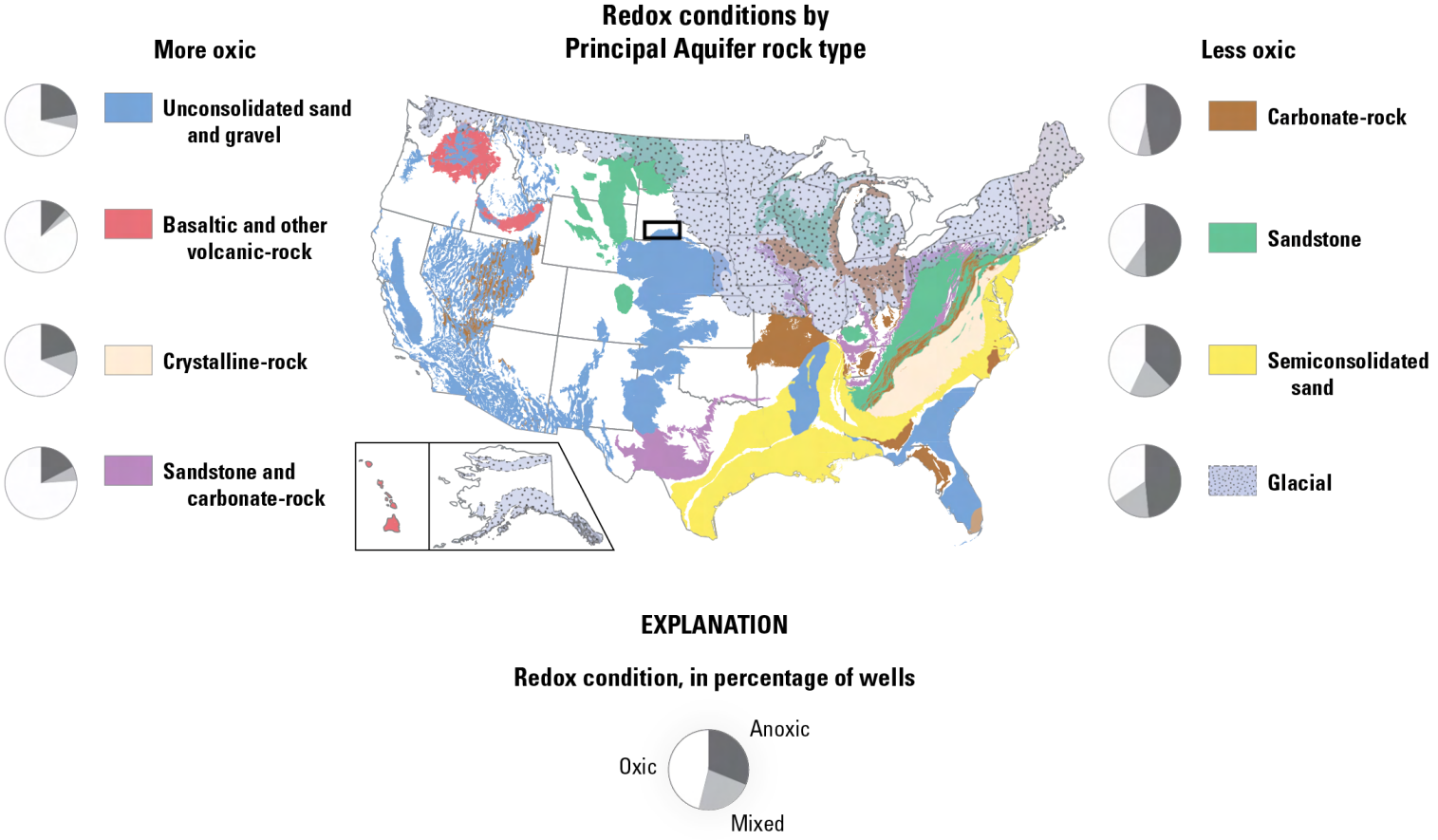

Figure 2.17: Redox conditions by principle aquifer rock type (Figure source: Resources (2019a)). Black box shows Pine Ridge Reservation study area. Edited by Jacob Abbott.

When comparing Figure 2.16 with my data (Figure 2.18) there is a clear difference in the observed trends. Rather than being separated into two distinct groups for arsenic and uranium (Figure 2.18) we see a clear linear relationship. With an R^2 of 0.79 there is a high level of correlation between these metals which is abnormal when seeing the predicted oxic mobilization trends (Figure 2.17). This suggests that an unexpected method of mobilization for arsenic or uranium is occurring. Due to the prevalence of oxic conditions in sand and gravel aquifers, arsenic is most likely being mobilized abnormally alongside normal oxic mobilization of uranium (Resources 2019a). One of the main methods this can occur is through the oxidative dissolution of arsenic-bearing sulfide minerals (Stolze, Battistel, and Rolle 2022). These equation:

$$Fe^{3+} + H_2O \leftrightarrow FeOH_2 + H^+$$

$$FeAsS + 2.75O_2 + 1.5H_2O \rightarrow Fe^{2+} + H_3AsO_3 + SO_4^{2-}$$

show the differences between the regular anoxic mobilization and the oxidative dissolution of arsenic (Stolze, Battistel, and Rolle 2022). In equation 2, sulfide-bearing minerals such as Arsenopyrite react with oxidized water to release the arsenic from the sediment. This arsenic releases in tandem with the uranium resulting in the positive trend seen in Figure 2.18.

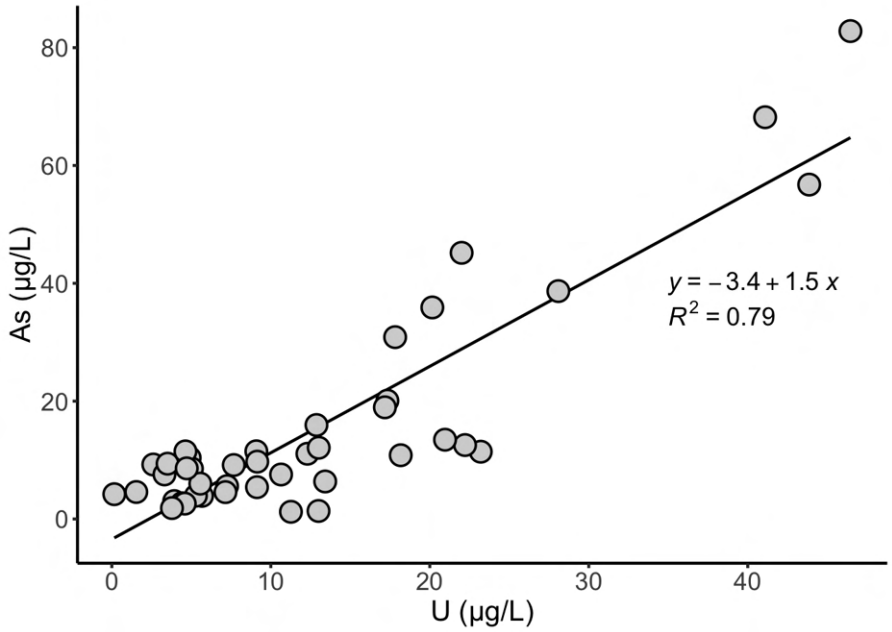

Figure 2.18: Scatter plot showing the correlation between arsenic and uranium. Data filtered to remove outlying arsenic value of 194.6 µg/L (See table above)).

Spatial Variability

Across the study area, there is notable spatial variability in arsenic and uranium surface water samples. When looking at dissolved arsenic concentrations in Figure 2.19 a few regions stand out. First is a grouping of low arsenic streams near the headwaters of the White River in upper Nebraska. This section has the lowest collective levels of arsenic on the White River with values averaging 3.6 µg/L and is also the farthest from the Pine Ridge Reservation. The next notable grouping is the high arsenic region near the Badlands National Park (Figure 2.1). These values of

dissolved arsenic were the highest observed in our study including the highest value of 194 µg/L. Across the central region of the Pine Ridge Reservation, we observe intermediate levels (4-14µg/L) of dissolved arsenic concentration. The commonality between these three groupings is their discharge into the White River.

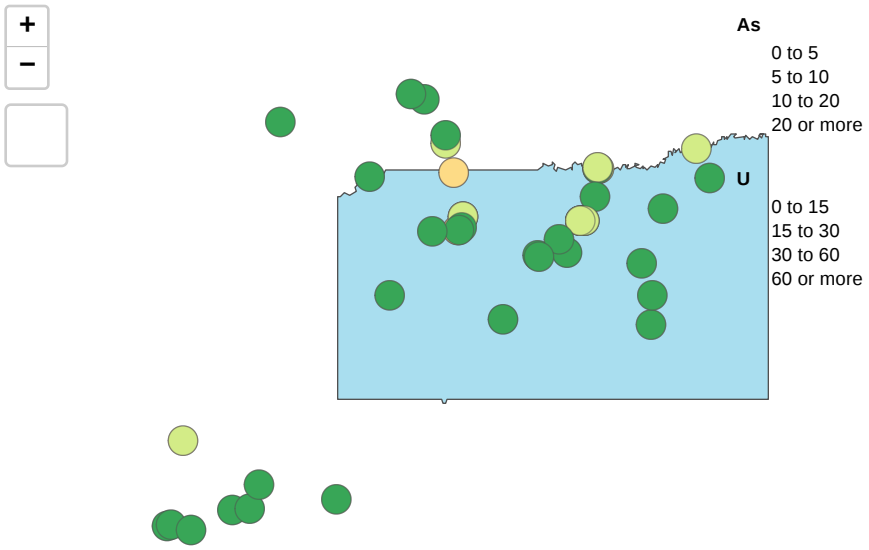

Figure 2.19: Map of study region with arsenic and uranium surface water samples. Source colors are based on the three sampling trips taken. Arsenic and uranium colors are based on the EPA guidelines of 10 for arsenic and 30 for uranium. Green shows values from zero to half the guideline, yellow shows values half the guideline to the guideline, orange shows from the guideline to double the guideline, red shows anything above the guideline. The blue square shows Pine Ridge Reservation. Use layers tab to switch between points and basemaps.

Using discharge area as a proxy of distance downstream we can single out changes in arsenic values as the stream flows (Figure 2.20). At the start arsenic levels are between 2 to 4 µg/L until the water flows into the reservation where it increases to 11 µg/L. This increase continues toward the Badlands where it increases up to 57 µg/L then peaks further downstream at 68 µg/L before dropping back down to 20 µg/L. While the general trend of increasing arsenic moving downstream is shown to be true the individual values may see large variability. The majority of the White River samples were taken in July 2021 and August 2022. These samples were both taken at the same time of year but were one year apart. This means while you would expect a similar general environment, the values we observed between the two were different with the 2022 sample having much higher concentrations of arsenic (Table 2.1). Looking at just the samples from their respective years they still show the low-high-mid trend described above (Figure 2.19). As compared to arsenic, concentrations of dissolved uranium on the map are less likely to exceed EPA guidelines with the majority of the locations falling under the low category (Figure 2.19). The few sampling locations that do show higher concentrations of uranium also follow the trend present in arsenic as confirmed by Figure 2.19.

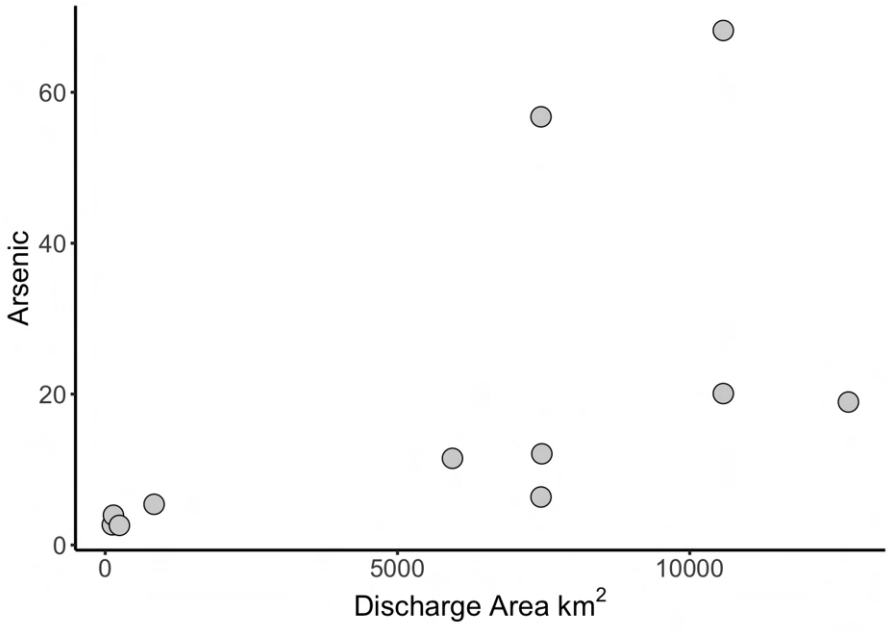

Figure 2.20: Stream water arsenic vs upstream drainage area.

Stable Water Isotopes

Local Stream Water Line

Water isotopes are a powerful tool capable of tracing water origin, hydrology, and climate effects. They are useful due to the water isotopes ^{18}O,^{17}O,^{16}O,^{2}H, and ^{1}H all being stable meaning they do not radioactively decay. Stable isotopes allow for accurate measures of stream water, groundwater, and precipitation as other than hydrological processes such as evaporation, precipitation, and mixing, the isotopes remain unchanged. Thus a sample once recharged into an aquifer will retain its isotopic condition as it moves along a flow path, absent any significant mixing. Isotopic

values also fall under predictable ranges geospatially. As seen in Figure 2.22 the δD and $\delta^{18}O$ values of groundwater for my study area and the rest of the US have been predicted (M. O. Stahl, Gehring, and Jameel 2020). Isotope values of precipitation allow for the creation of the Global Meteoric Water Line (GMWL). The GMWL, seen as the black dashed line in Figure 2.21, shows the global relationship between these aforementioned hydrogen and oxygen isotopes and can be defined using the equation (Craig 1961):

\begin{equation} δD=8×δ^{18}O+10 \tag{2.3} \end{equation}

Looking at the data in Figure 2.21, we can see that our points do not follow the same slope as the GMWL. This is to be expected as Local Meteoric Water Lines (LMWL), the functional relationship between these isotopes on a local scale, often departs from the GMWL (Tappa et al. 2016). However, by definition, the LMWL refers to meteoric water and since our samples are primarily surface water we will be using LSWL (Local Surface Water Line). In the figure we see that the LSWL is defined by the equation:

\begin{equation} y = 5.986x - 24 \tag{2.4} \end{equation}

The LSWL has an R^2 value of 0.98 and a slope of 5.986 which is shallower than the GWML of 8. The degree to which this LSWL varies off the GMWL is useful as it can reveal important information about meteoric sources and atmospheric conditions of the water (Tappa et al. 2016).

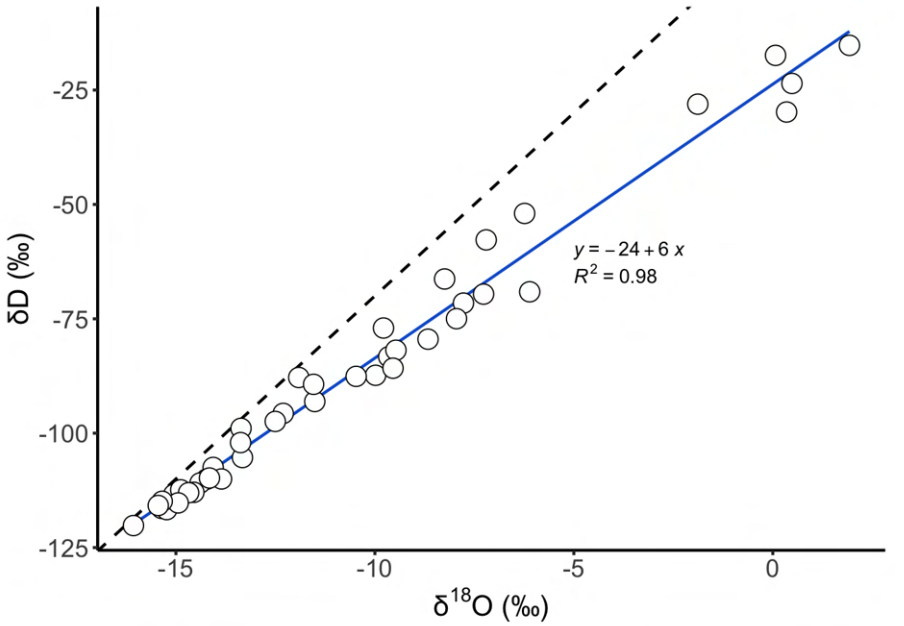

Figure 2.21: Scatter plot between $\delta^{18}O$ and δD of stream water samples. Local Stream Water Line in blue. Global Meteoric Water Line in black

Spatial Variability

The spatial variation of isotopes across the US is a widely studied topic with many predictive models being made (M. O. Stahl, Gehring, and Jameel 2020). As seen in Figure 2.22, the region of South Dakota containing our study area has a large range of isotopic variation in groundwater, stream water, and precipitation compared to the rest of the state. This variation is caused by a few factors, the foremost being evaporation and condensation. When water evaporates from a body of water, most commonly the ocean, lighter isotopes (^{16}O and ^{1}H) preferentially evaporate causing more heavy isotopes (^{18}O and ^{2}H) to be left behind (Friedman et al. 1964). Furthermore, heavy isotopes also preferentially precipitate resulting in the remaining atmospheric water vapor becoming isotopically lighter as air masses move inland (Friedman et al. 1964). This results in the distribution of groundwater isotopes across the US looking similar to the groundwater model in Figure 2.22 (M. O. Stahl, Gehring, and Jameel 2020). By comparing the stream water isotopes measured in this study to the predicted groundwater isotopes at those locations we find that on this map we can see that some sampling locations have an isotopic composition similar to the local groundwater however many did not. Samples where stream water isotopes differ from the groundwater isotopes suggest that the stream water may have alternative sources or processes like evaporation may have occurred.

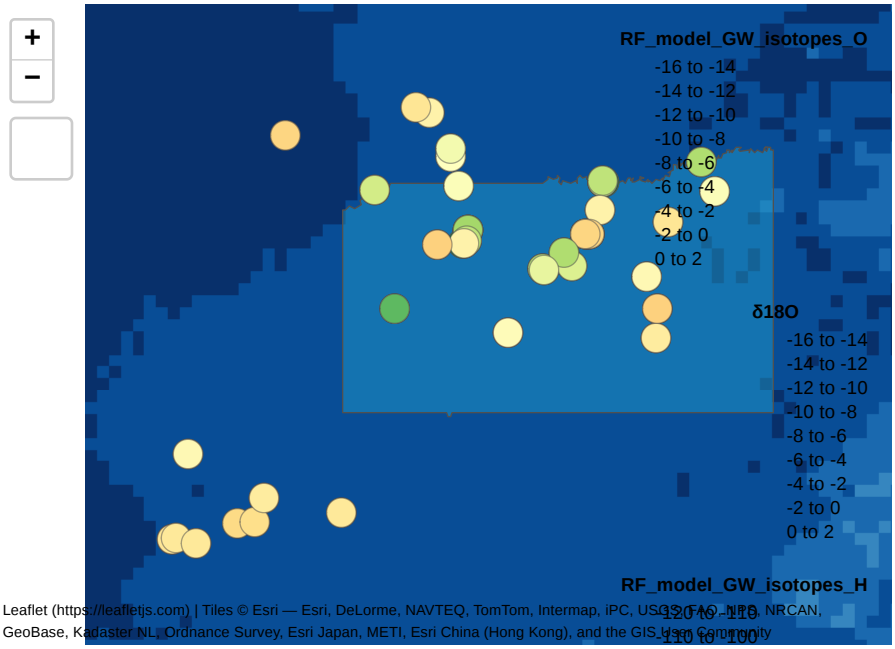

Figure 2.22: Map of Pine Ridge Reservation points with groundwater isoscapes from M. O. Stahl, Gehring, and Jameel (2020).

Deuterium Excess

Deuterium excess (d-excess) provides valuable information which can be used to help determine the source and evolution of moisture during transport (Bershaw 2018). D-excess is defined as:

$$\text{d-excess} = \delta D - 8 \times \delta^{18}O \tag{2.5}$$

and shows the influence of temperature and relative humidity on the water at its source location (Dansgaard 2012). D-excess is also strongly influenced by evaporative processes with evaporation at humidity below 100% (kinetic fractionation) resulting in an increase in d-excess of the vapor (relative to the liquid water it evaporated from) and a decrease in the d-excess of the remaining water in the liquid phase (Marshall, Brooks, and Lajtha, n.d.). In Figure 2.23 the effects of kinetic fractionation can be seen as the points farther off the GMWL (lighter coloring) imply $\delta^{18}O$ is more enriched (Marshall, Brooks, and Lajtha, n.d.). Since this fractionation happens during evaporation we can make the conclusion that evaporation must have occurred to the surface water at these sample sites. The effects of this evaporation can also be seen in Figure 2.22 where the isotope points with the highest variation from the predicted map values also have the highest d-excess.

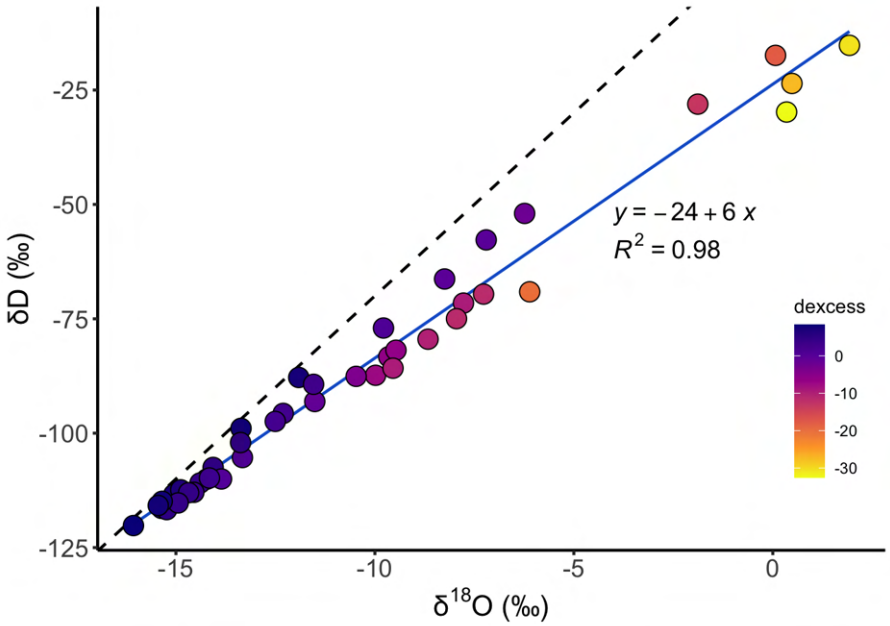

Figure 2.23: Scatter plot between $\delta^{18}O$ and δD stream water samples colored by D-excess. Local Stream Water Line in blue. Global Meteoric Water Line in black.

$\Delta^{17}O$

Similarly to d-excess, $\Delta^{17}O$ is a second-order parameter used to understand the evolution of moisture during transport. It is defined by the equation:

$$\Delta17O = \ln\left(\frac{\delta^{17}O}{1000} + 1\right) - 0.528 * \ln\left(\frac{\delta^{18}O}{1000} + 1\right) \tag{2.6}$$

which is the deviation from a reference relationship between $\delta^{18}O$ and $\delta^{17}O$ (Bershaw, Hansen, and Schauer 2020). The main difference between $\Delta^{17}O$ and d-excess is that $\Delta^{17}O$ is only a function of temperature while d-excess is a function of both temperature and humidity (Affolter et al. 2015). As seen in Figure 2.24, there is a similar relationship to what is seen with d-excess (figure X) but with some more variation. This variation has a number of possible causes but the most probable is the poor calibration of $\delta^{17}O$ standards.

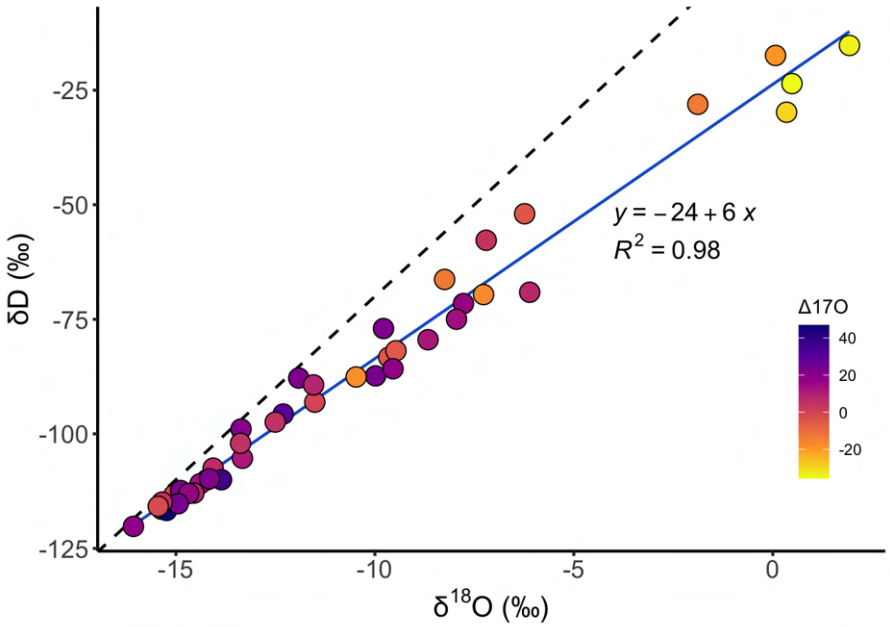

Figure 2.24: Scatter plot between $\delta^{18}O$ and δD colored by $\Delta^{17}O$. Local Stream Water Line in blue. Global Meteoric Water Line in black.

Isotopes and Contaminants

Relationships

Arsenic, uranium, and isotopes all have correlations between themselves but the relationships between these metals and isotopes are relatively unstudied. To better understand the simultaneous mobilization of both arsenic and uranium as well as the effects caused by climate and transportation through water, understanding isotopes under these conditions is important. Taking a look at the correlation between $\delta^{18}O$ and δD (Figure 2.25) we can see that it resembles the similar plot made above colored by d-excess (Figure 2.23). By plotting both arsenic and d-excess vs each other we can see that there is a weak negative trend with an R^2 of 0.48 (Figure 2.26). On this figure two probable grouping of samples stand out. The first group of samples has high d-excess and low arsenic. The other group of samples has much lower d-excess that decreases variably in relation to increasing arsenic.

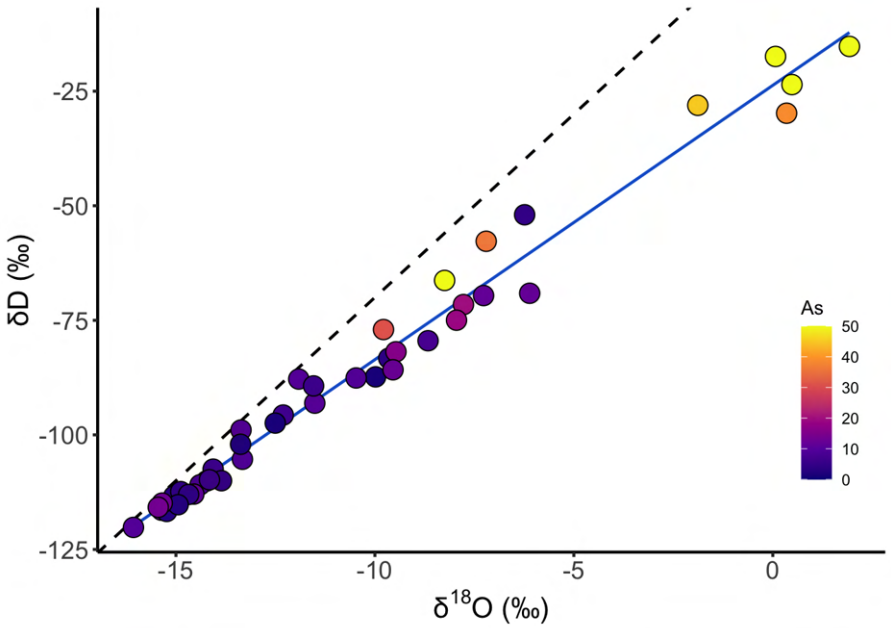

Figure 2.25: Scatter plot between $\delta^{18}O$ and δD colored by Arsenic. Local Stream Water Line in blue. Global Meteoric Water Line in black.

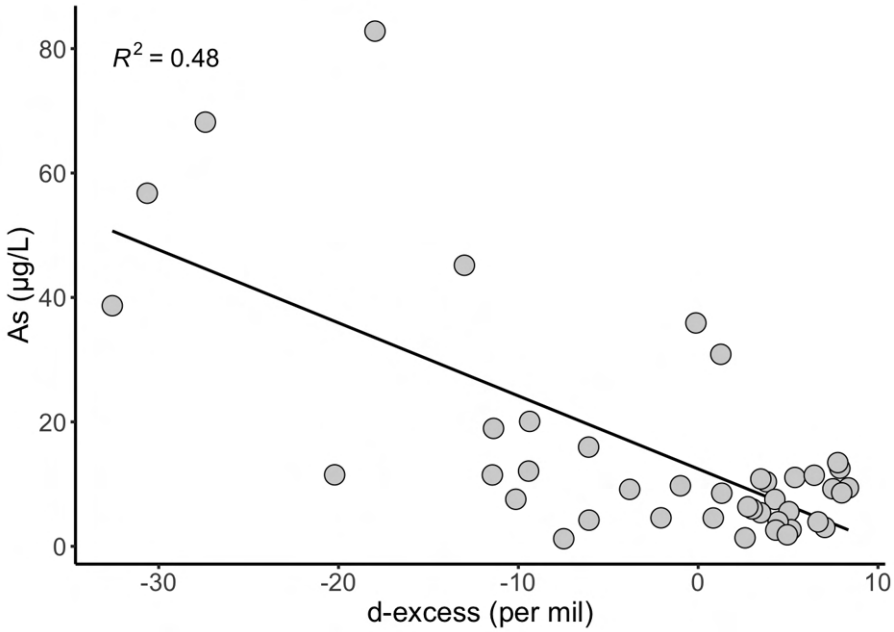

Figure 2.26: Stream water arsenic vs d-excess. Blue shows d-excess less than 0 and green shows d-excess greater than 0. Y axis fit to remove extreme high arsenic outlier.

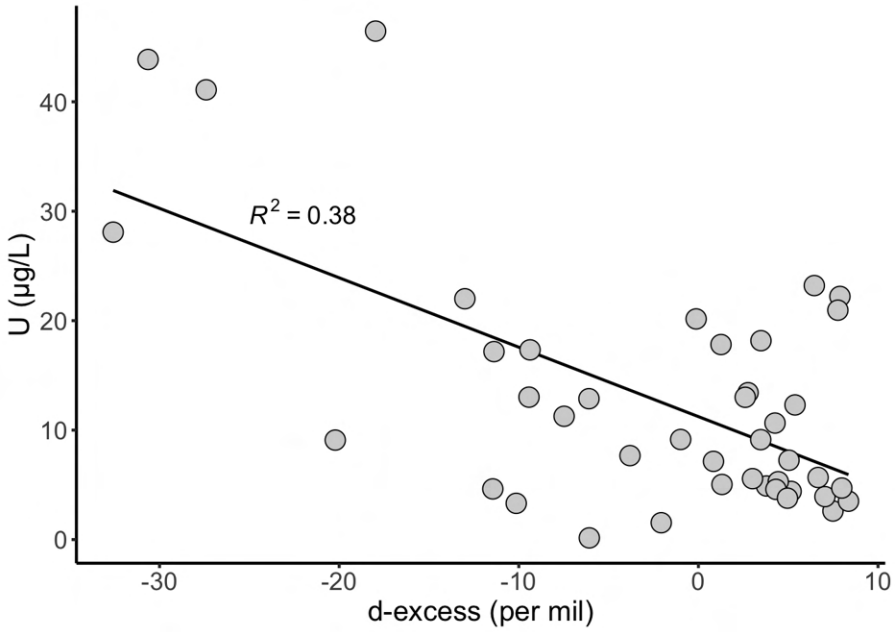

Figure 2.27: Stream water uranium vs d-excess. Blue shows d-excess less than 0 and green shows d-excess greater than 0. Purple shows potential outlier. Y axis fit to remove extreme high arsenic outlier.

The two groups appear to break right around the d-excess value of zero so I grouped the two and fit a linear model to each. The first group of samples has slight positive slope but a very weak R^2 with a value of 0.14 and the other group has larger negative slope and an R^2 of 0.49. By comparing these two groups we can see that they are significantly different however the second groups R^2 of 0.49 is not significantly different than the collective R^2 of 0.48. To better understand the high and low d-excess groups I created a scatter plot between arsenic uranium and $\delta^{18}O$ (Figures 2.28 and 2.29). Between these figures and the original (Figure 2.26) there were some abnormalities. The main abnormality is three samples (including the high arsenic outlier in Table 2.2) with high arsenic values and near zero d-excess values (Figure 2.26). These three samples (two in Figure 2.28) are highlighted in purple and were categorized as possible outliers (Figure 2.28 and 2.29). The remaining samples are grouped in to high d-excess (green) and low d-excess (blue).

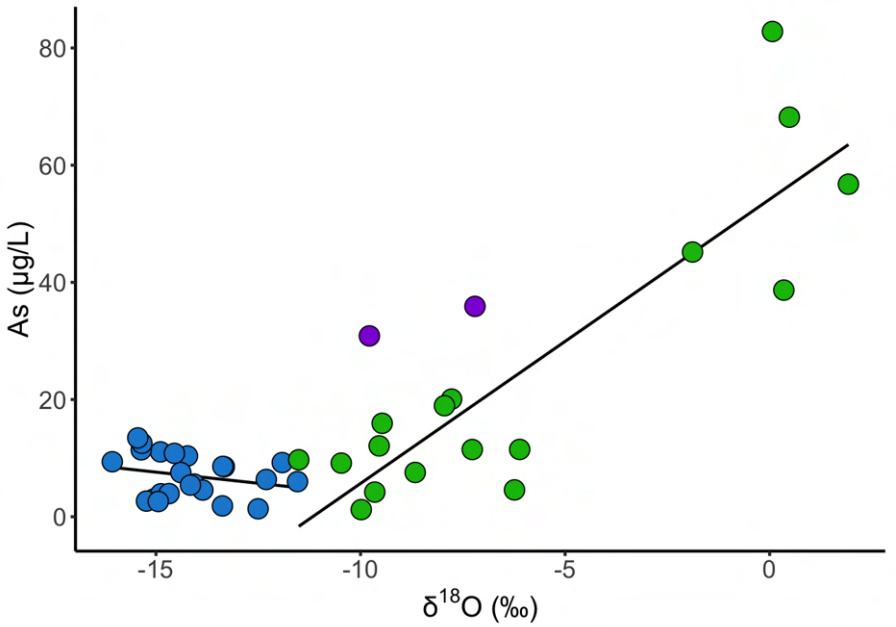

Figure 2.28: Arsenic vs $\delta^{18}O$ grouped by d-excess. Blue shows d-excess less than 0 and green shows d-excess greater than 0. Purple shows potential outlier (i.e. Arsenic concentration are greather than expected based on isotopic compositions). Y axis fit to remove extreme high arsenic outlier.

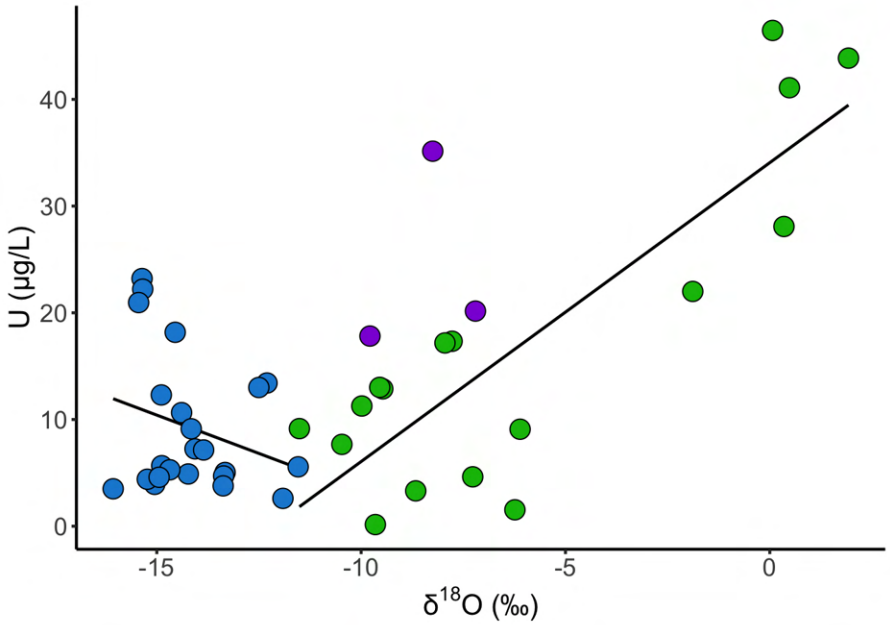

Figure 2.29: Uranium vs $\delta^{18}O$ grouped by d-excess. Blue shows d-excess less than 0 and green shows d-excess greater than 0. Purple shows potential outlier (i.e. Uranium concentration are greather than expected based on isotopic compositions).

In both figures (Figures 2.28 and 2.29) the clear groupings (green) of lower arsenic high d-excess points that don't have a noticeable trend. Both had insignificant R^2 values of 0.064 and 0.073. The high arsenic low d-excess group (blue) however had a noticeable R^2 of 0.77 and 0.72. This strongly suggests two possible conclusions. First is that as arsenic and uranium increase, d-excess decreases. A possible reason for this is d-excess being strongly influenced by evaporative effects (Marshall, Brooks, and Lajtha, n.d.). This is likely the driving factor however water source and precipitation may also play a role. The second conclusion than can be proposed is the idea that there is a minimal relationship between arsenic and uranium in our surface water samples compared to isotopes when d-excess changes are not present.

Outliers

There were three notable outliers observed in the data and analysis. The first was point BB08 which has an extremely high arsenic concentration of 194.6 µg/L. It was removed from almost all figures as it caused the map scales to be abnormal. This includes the arsenic vs uranium plot (Figure 2.18) as while the uranium value was high as 35.1 µg/L it fell well within the expected range of values unlike the arsenic value. Using our slope equation:

$$y = -3.4 + 1.5x \tag{2.6}$$

from Figure 2.18 and our uranium value of 35.1 µg/L we would expect to see an arsenic value of 49.25 µg/L. This is 159.5 µg/L below what we actually see suggesting that this is in fact an outlier and there is a separate source responsible for the variation. The other outliers can be seen as the purple points in Figure 2.28. These sites (ND_WC1 and BB09) seemed to have normal metal concentrations compared to other points but have a positive d-excess of 1.258 and a near zero d-excess of -0.128. One notable trait these two samples have is a large difference between As and U. In Figure 2.30 below we see the difference between As and U plotted against $\delta^{18}O$ similar to Figure 2.28. In the plot we see the potential error points (blue) having a relatively normal difference compared to other points however they have a much lower $\delta^{18}O$ than their counterparts. This combined with close to zero d-excess' leads me to believe that there is an external source responsible for the variation.

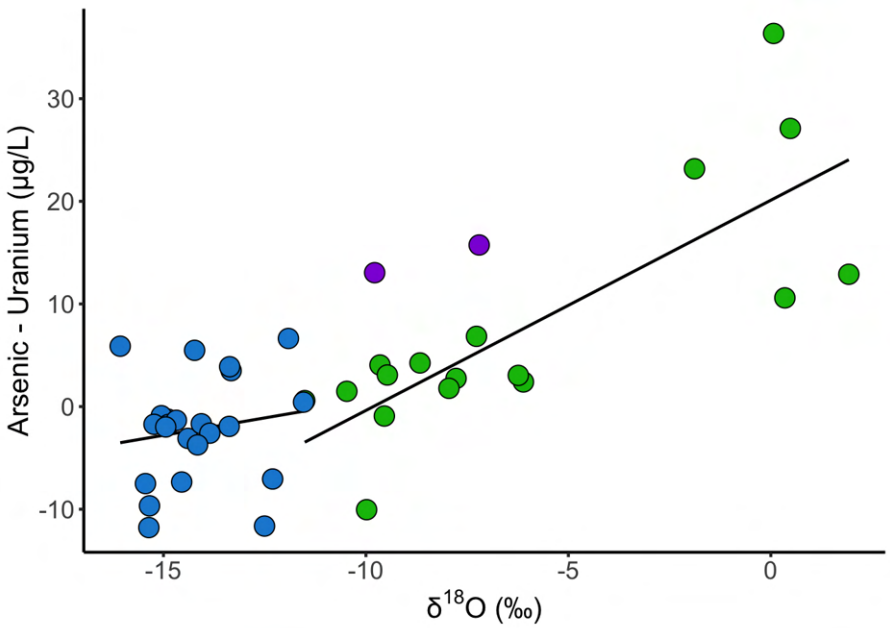

Figure 2.30: Difference between arsenic and uranium vs $\delta^{18}O$ grouped by d-excess. Blue shows d-excess less than 0 and green shows d-excess greater than 0. Purple shows potential outlier. Y axis fit to remove extreme high arsenic outlier.

One potential cause of the variation seen in all three points is their spacial location. The map below (Figure 2.31) highlights just these points and one observable feature present at all three is sandy white colored terrain. For points BB08 and BB09 this is the Badlands National Park (Figure 2.1) and for ND_WC1 this is the Toadstool Geological park. This spatial correlation suggests that the terrain present in each reason is a possible cause of elevated arsenic concentration above normal regional concentrations

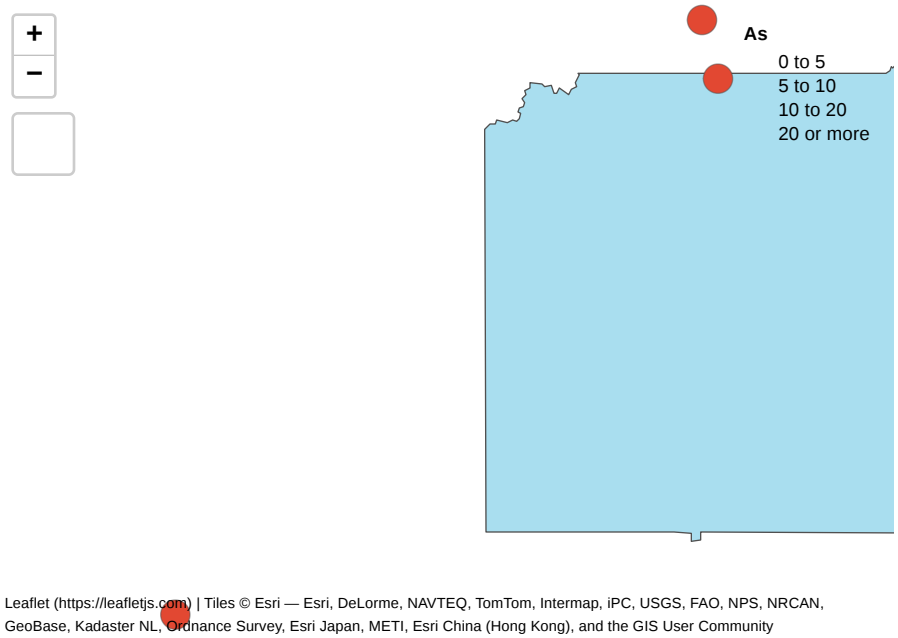

Figure 2.31: Map of potential outliers.

2.5.0.1 **Other Metals**

To better understand if evaporation is the main cause of arsenic enrichment we can look at other elements in the samples to see if they share a similar relationship with arsenic. One element useful for this is sodium as it is minimally impacted by external sources once dissolved. To do this we can compare concentrations of both arsenic and sodium at sample location with multiple sample times to see if they remain proportional. By plotting this we cans see that arsenic and sodium do remain proportion at each source (Figure 2.32). Additionally, multiple location also share a similar linear trend further showing the relationship. We can also see that in these location groupings d-excess also increases proportionally to sodium (Figure 2.34). By comparing Figures 2.33 and 2.34 this trend is further strengthened as arsenic and sodium both show near identical trends. This strongly supports that the main cause for enriched arsenic and uranium in our study area is in fact primarily due to evaporation.

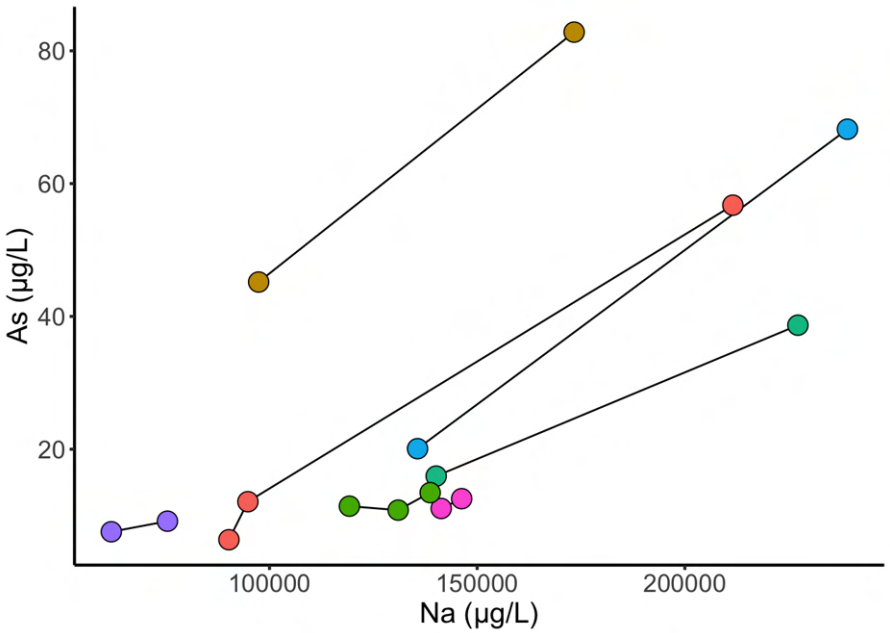

Figure 2.32: Arsenic vs sodium grouped and colored by sampling location.

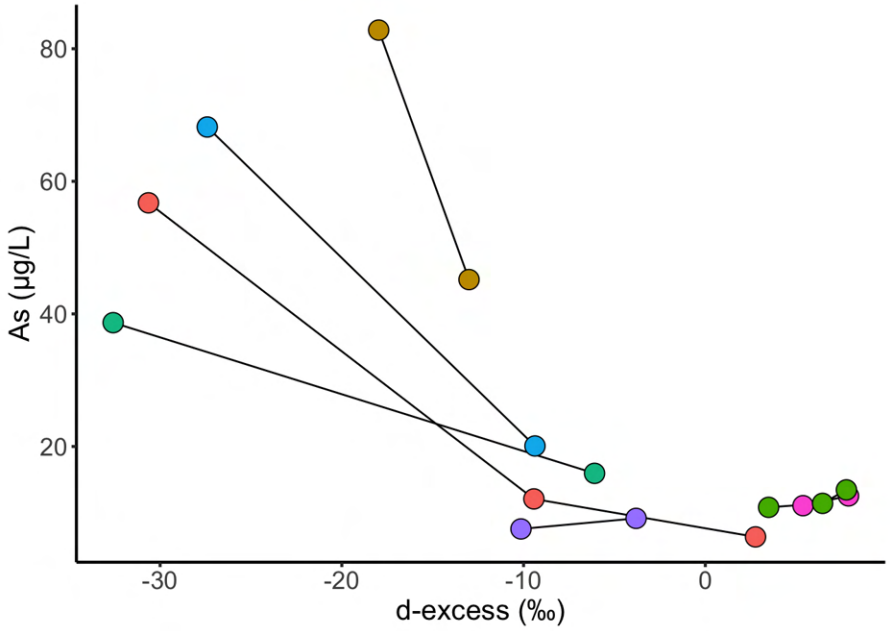

Figure 2.33: D-excess vs arsenic grouped and colored by sampling location.

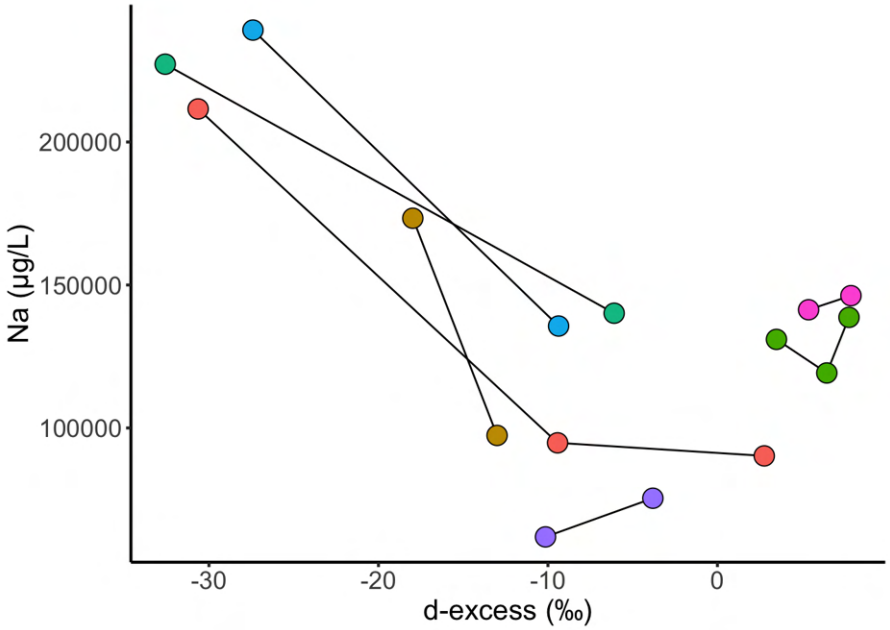

Figure 2.34: D-excess vs sodium grouped and colored by sampling location.

3 Characterizing Arsenic and Uranium Contamination through Isotopic and Hydrologic Inference

3.1 Introduction

Groundwater is a vital natural resource stored in aquifers in the subsurface across the globe. However, understanding this typically invisible resource is difficult as collecting samples on a large scale is not easily achievable (Lall, Josset, and Russo 2020). To understand hydrological processes and manage groundwater resources, it is important to determine the sources of water contributing to the region through the use of precipitation and stream water (Gonzales et al. 2009). One way to quantify groundwater's contribution is by using samples of local stream water. Stream samples generally contain a mix of both precipitation, in the form of runoff from storm events, and groundwater from aquifer baseflow (Freeze 1974). For streams where baseflow is the principal component contributing to stream flow, increased rates of groundwater extraction through pumping during periods of limited precipitation can significantly reduce stream flow. Therefore, proper management of surface water and groundwater resources is imperative for the sustainability of these resources for future generations.

Determining the relative contributions of surface runoff from precipitation and groundwater to stream flow can be accomplished by measuring the hydrogen and oxygen isotopes of water ($^{18}O/^{16}O$ and $^{2}H/^{1}H$). Hydrogen and oxygen isotope ratios in water can be used as tracers for water sources and water circulation in the environment (Fry 2006). Stable isotopes can be useful tools to understand the movement of water through various reservoirs, including evapotranspiration, groundwater recharge, and runoff (Jung et al. 2020). Due to precipitation being the principal source of water to watersheds, hydrogen and oxygen isotopes in precipitation are often studied in hydrological investigations (Vreča and Kern 2020). In a recent study stable isotopes were analyzed in water to determine whether streams were sampled under baseflow conditions (M. Stahl et al. 2021). Their results suggest that groundwater was contributing the most to stream flow during the study interval (Figure 3.1). In the figure, we can see a large range of precipitation values (blue circles) compared to both our ground and stream water average values (green square and grey circle). The likely reason for this is the long-term accumulation and mixing of seasonal precipitation in groundwater and the short-term impact of precipitation on stream water resulting in both values being close to a yearly average of all monthly samples.

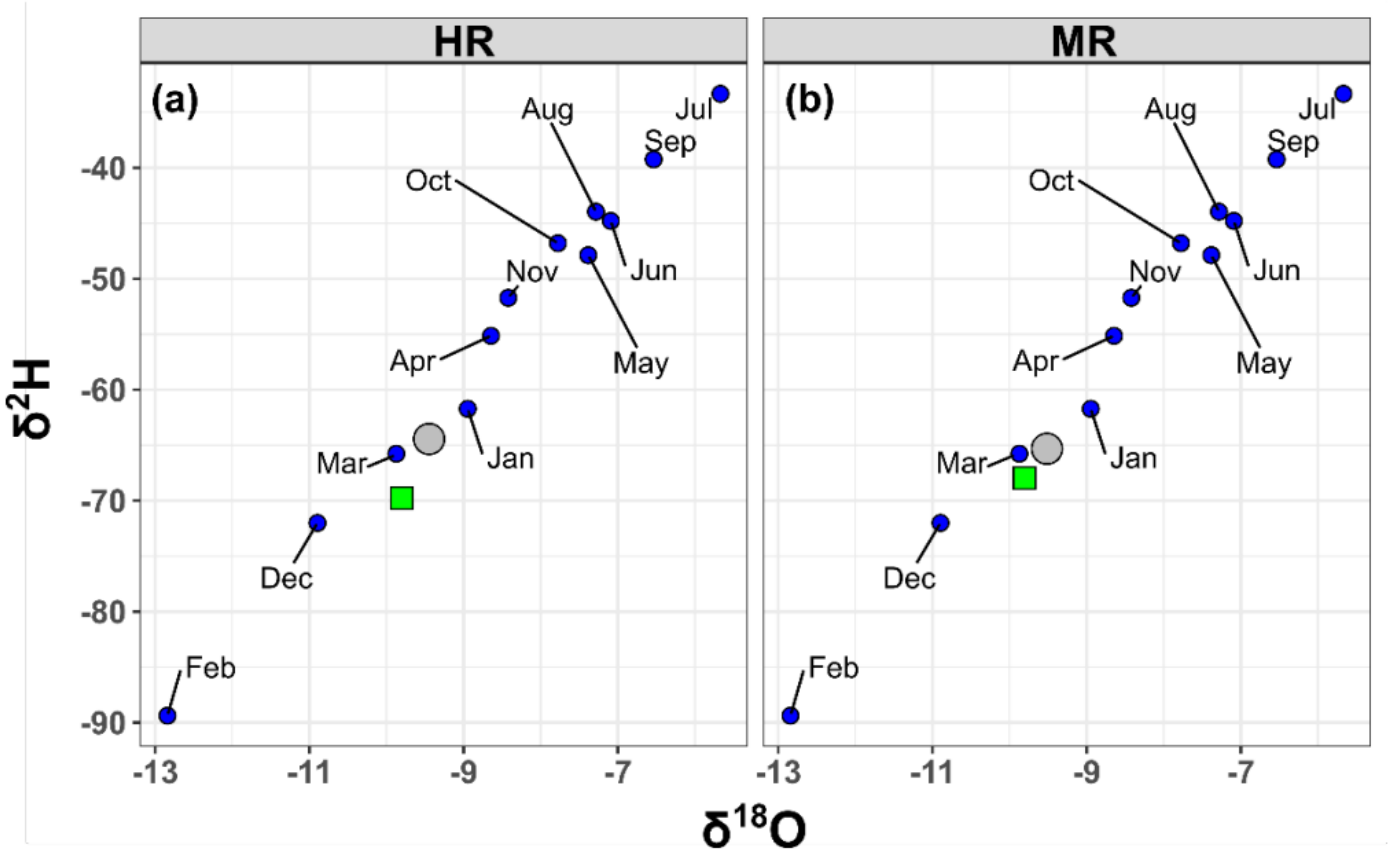

Figure 3.1: Relationship between $\delta^{18}O$ and δD of river water from the Hudson River (left panel) and the Mohawk River (right panel) (Figure source M. Stahl et al. (2021)). The measured H and O isotopes in each river (grey circles) and modeled groundwater isotopes (green squares) are shown. Weighted mean monthly precipitation isotope values are also shown (blue circles). The precipitation samples were collected in 2016-2021 from Schenectady and Little Falls, NY.

In the Pine Ridge Reservation study area, we are interested in understanding the fractional contributions of both groundwater and precipitation to our surface water samples to determine the dominant flow path of arsenic and uranium. To achieve this goal we will be using a mixing model with our precipitation and groundwater end members to deduce source predominance in the study area. We hypothesize (1) that groundwater will be the dominant source of stream flow during the winter and summer, and (2) high arsenic and uranium location will be seen in groundwater dominant locations.

3.2 **Methods**

Due to multiple sources of water that contribute to the stream flow in the study area, it was necessary to use a mixing model to separate the different components contributing to stream flow. This approach involves using the isotope values of two isotopic signatures and their fractional contributions to quantify the source contributions to a mixture (Phillips, Newsome, and Gregg 2005). We implemented this approach using the equations:

$$\delta^{18}O_{stream\ water} = \delta^{18}O_{groundwater}(f_{groundwater}) + \delta^{18}O_{precipitation}(1 - f_{groundwater}) \tag{3.1}$$

$$f_{groundwater} = \frac{(\delta^{18}O_{stream\ water} - \delta^{18}O_{precipitation})}{(\delta^{18}O_{groundwater} - \delta^{18}O_{precipitation})} \tag{3.2}$$

$$f_{precipitation} = 1 - f_{groundwater} \tag{3.3}$$

where $f_{groundwater}$ is the fractional component of groundwater contributing to stream flow. Using equation 11 $f_{streamwater}$ can be calculated using $f_{groundwater}$. As we only measured stream water values, ground water $\delta^{18}O$ values were collected from a groundwater isoscape and precipitation $\delta^{18}O$ values were collected from a precipitation isoscape (M. O. Stahl, Gehring, and Jameel 2020; Bowen 2023). As samples were taken in different months precipitation isotopes were taken from the average isoscape values in each month. A single value was used for groundwater as it is less susceptible to short-term seasonal changes.

3.3 **Results**

Table 3.1: Predicted fraction groundwater (baseflow) for each sampled stream. Column 'Fraction Groundwater' is based of predicted groundwater isotopes at each site. Column 'Fraction Ground Prediction' is based on the use of the $\delta^{18}O$ endmember of -16‰. Fractional compositions should range between 0 and 1, with zero indicating stream water is composed of exclusivly precipitation and 1 indication stream water is composed exclusivly of groundwater. Values avobe and below the 0 to 1 range indicate stream water isotopes that fell outside the two end member mixing model.

Location	Date	δ18O(‰)	Arsenic(µg/L)	Uranium(µg/L)	Dexcess	Fraction Groundwater	Fraction Ground Prediction
CY1	2022-08-13	-9.983	1.220520	11.265000	-7.477	0.4757810	0.3583292
PC1	2022-08-13	-14.890	11.071680	12.301080	5.378	1.2350332	0.8864866
CC1	2022-08-13	0.069	82.813840	46.458800	-17.973	-0.8703956	-0.6514608
BC1	2022-08-13	-11.914	9.245979	2.609171	7.490	0.5733456	0.5189764
LD1	2022-08-13	0.347	38.677200	28.086780	-32.582	-0.7821808	-0.5668860

Location	Date	δ18O(‰)	Arsenic(µg/L)	Uranium(µg/L)	Dexcess	Fraction Groundwater	Fraction Ground Prediction
MR1	2022-08-13	-8.664	7.562986	3.311101	-10.143	0.3487527	0.2582508
WR1	2022-08-13	-6.110	11.490110	9.089861	-20.217	0.0065146	0.0048523
WR3	2022-08-13	1.926	56.756450	43.864340	-30.639	-1.1316848	-0.8466454
WR5	2022-08-13	0.481	68.193620	41.093490	-27.405	-0.8008511	-0.5803266
ND_BC1	2021-07-01	-14.231	10.377650	4.896757	3.790	1.1708785	0.7996164
ND_BC2	2021-07-01	-13.329	8.536609	5.036722	1.311	1.0474801	0.7111948
ND_CBR1	2021-07-01	-15.053	3.036608	3.923925	7.044	1.2061546	0.8867324
ND_CBR2	2021-07-01	-14.880	3.924991	5.672967	6.662	1.1729859	0.8699269
ND_CC1	2021-07-01	-1.885	45.176680	22.001780	-13.002	-0.7299201	-0.5356714
ND_CCR	2021-07-01	-14.394	7.551520	10.645600	4.264	1.1240452	0.8132959
ND_CVC1	2021-07-01	-14.065	5.574549	7.248261	5.042	1.1444622	0.7885877
ND_PAC1	2021-07-01	-11.511	9.730366	9.147527	-0.989	0.7279054	0.5341916
ND_PC1	2021-07-01	-9.652	4.207683	0.155147	-6.074	0.4158319	0.2975862
ND_PC2	2021-07-01	-15.361	11.419550	23.206460	6.452	1.3464800	0.9243125
ND_PC3	2021-07-01	-14.550	10.821970	18.171250	3.482	1.2200045	0.8374914
ND_PC4	2021-07-01	-9.471	15.949120	12.871620	-6.094	0.4510351	0.3162310
ND_PCQ1	2021-07-01	-13.855	4.556893	7.146385	0.838	1.0483940	0.7556622
ND_WC1	2021-07-01	-9.784	30.865350	17.820070	1.258	0.4235949	0.3215603
ND_WM1	2021-07-01	-16.068	9.389835	3.506099	8.355	1.4625685	1.0000000
ND_WR1	2021-07-01	-15.233	2.675883	4.403090	5.161	1.1757078	0.9069046
ND_WR2	2021-07-01	-14.681	3.952064	5.287716	4.444	1.0958569	0.8454439
ND_WR3	2021-07-01	-14.944	2.603147	4.588096	4.317	1.1435316	0.8755060
ND_WR4	2021-07-01	-14.158	5.399254	9.130444	3.469	1.0611359	0.7926842
ND_WRB1	2021-07-01	-7.774	20.076770	17.333870	-9.373	0.2001640	0.1403395
ND_WRB10	2021-07-01	-7.949	18.953930	17.174350	-11.381	0.2418648	0.1761584
ND_WRB2	2021-07-01	-9.545	12.092860	13.013020	-9.432	0.4012481	0.2947817
BB01	2021-12-01	-11.541	5.999025	5.565706	3.013	1.3206465	3.0669852
BB02	2021-12-01	-15.345	12.547013	22.215756	7.878	0.5769068	1.3164636
BB03	2021-12-01	-15.445	13.455723	20.958169	7.763	0.5565747	1.2743171
BB04	2021-12-01	-7.269	11.473231	4.629525	-11.447	2.1645664	4.3443008
BB05	2021-12-01	-10.471	9.157387	7.669545	-3.809	1.5615008	3.0246210
BB06	2021-12-01	-12.304	6.364771	13.420011	2.763	1.2484264	2.3357951
BB07	2021-12-01	-13.365	8.595087	4.709632	7.982	1.0564663	1.8600313
BB08	2021-12-01	-8.248	194.672932	35.144018	-0.312	2.0324054	3.7139639
BB09	2021-12-01	-7.203	35.904088	20.159527	-0.128	2.2204391	3.9717505
BB10	2021-12-01	-6.237	4.579357	1.538960	-2.070	2.3907383	4.3103496
BB11	2021-12-01	-12.504	1.360328	13.000881	2.606	1.2460462	2.2568030
BB12	2021-12-01	-13.376	1.851737	3.782120	4.957	1.0604962	1.9269077

3.4 **Discussion**

Mixing Model

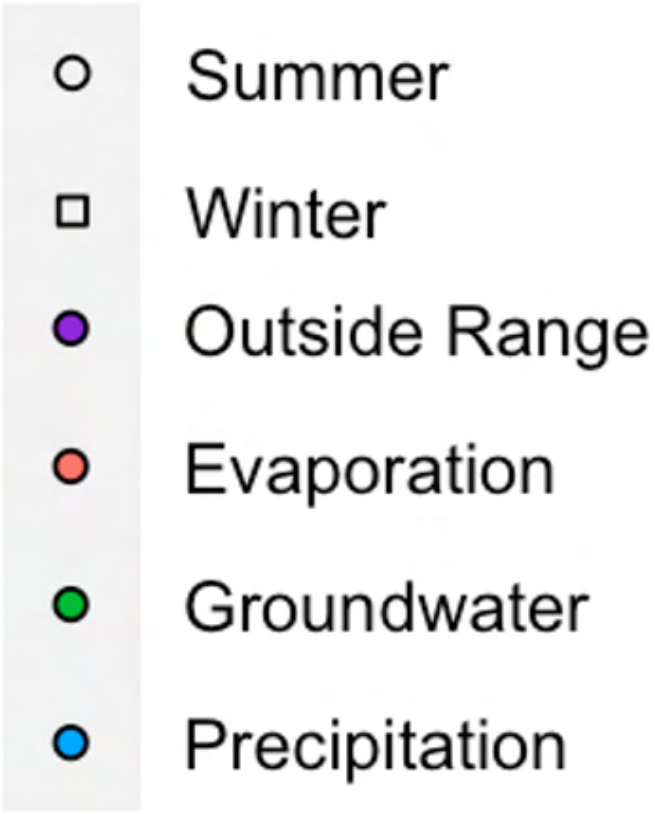

Figure 3.2: Section Key

After completing a mixing model using the equations above (Equation (3.1), (**ref?**)(eq:f2), and (**ref?**)(eq:f3)) we would expect all samples sites to fall between the range 0 to 1. This represents the proportion of the water that came from each source where values between 0 and 0.5 are primarily consistent of precipitation and values between 0.5 and 1 are primarily consistent of groundwater. Using our groundwater end member value of about -13.5‰ and our seasonal precipitation values of about -6‰ for July and August (summer) and about -18.5‰ for December (Winter) points fell in to three groups (Table 3.1 and Figure 3.3). The first two groups were precipitation (blue) and groundwater (green) which were expected based on our fractionation equation (Equation (3.1)). However, a majority of our points fell outside the bounds of 0 and 1 and were marked as temporary errors (red and purple). The first possible explanation for unexpected variation between samples is the previously mentioned seasonal differences. As we saw in the supplementary figure above monthly samples have large seasonal variations (M. Stahl et al. 2021). This is also the case in our study area as July and August end member, referred to hereafter as summer, and December end member, referred to hereafter as winter, fall on either side of the groundwater end member. To account for this each season will be analyzed separately.

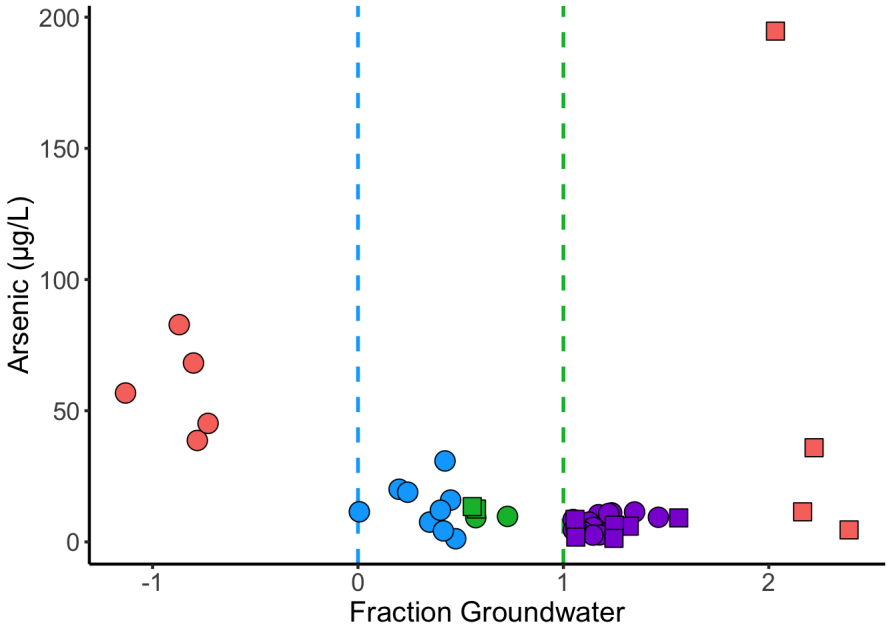

Figure 3.3: Streamwater samples percent groundwater vs. arsenic grouped by water source composition (eg. Groundwater vs precipitation). Blue line shows 100% precipitation, green line shows 100% groundwater. Blue points show precicipitation dominance, green points show groundwater dominance, purple and red points show samples that fall outside the mixing model. Squares represent winter samples and circles represent summer samples.

Summer

One notable feature present is the large grouping of errors just above 100% groundwater (purple) which suggests the error may not be due to random variation (Figure 3.3). A possible cause for these points having a higher than 100% proportion of the groundwater is that the groundwater end member may be inaccurate. This is possible as the region around The Pine Ridge Reservation has many isotopic changes over a short distance compared to the rest of the United States. Looking at our summer values one point stands out with the lowest $\delta^{18}O$ of -16.068‰ (Figure 3.4).

After taking a closer look this sample is SD_WM1 (Table 3.1) which was a surface water windmill sample. However, since it was next to a windmill it was likely a groundwater sample pumped to the surface. By using -16.068‰ as our groundwater end member (red line below) instead of our location based values of about -13.5‰ (blue line below) we see that our points fit much better between our two new endmembers (Figure 3.4). This removes the entire grouping of error points (purple) and better shows the proper fraction of both precipitation and groundwater (Figure 3.5).

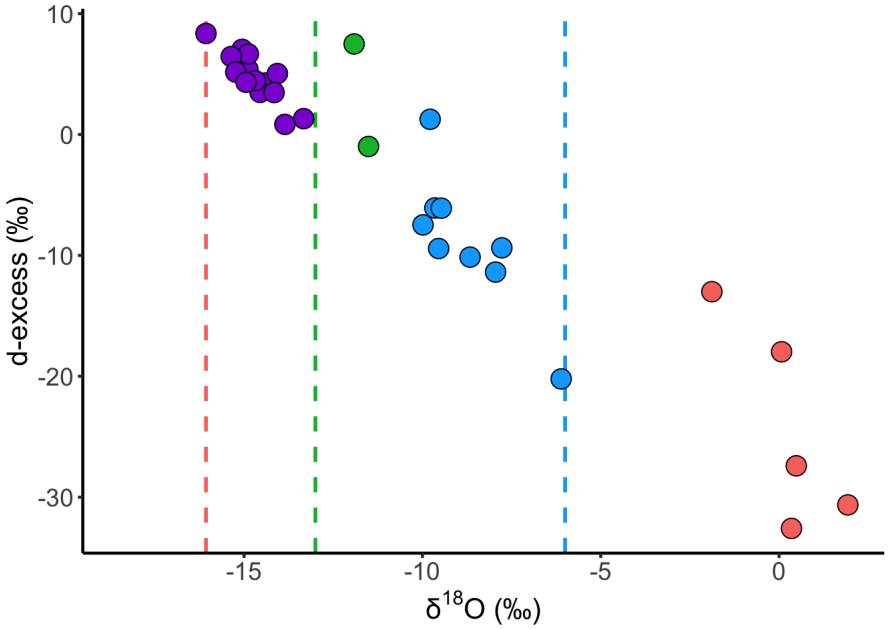

Figure 3.4: D-excess vs. $\delta^{18}O$ grouped for summer samples by water source composition (eg. Groundwater vs precipitation). Blue line shows precipitation endmenber, green line shows groundwater endmember, and red line shows new groundwater endmember. Blue points show precicipitation dominance, green points show groundwater dominance, purple and red points show samples that fall outside the mixing model.

The remaining red error points can be more easily explained. Looking at Figure 3.5 we can see that they have a below zero proportion of groundwater or in other words are more than 100% precipitation. This is abnormal as July an August have the highest possible isotopic values. Being above these values implies that an external source other than groundwater and precipitation caused that change. By comparing these points to other metrics we can see that they have very low d-excess values (Figure 3.4) as well as very high arsenic values (Figure 3.5). As discussed in Chapter 2, these two factor were found to be a sign of high evaporation. Since evaporation causes fractionation and enrichment of $\delta^{18}O$ we can conclude that these points don't fit the predicted mixing model due to evaporative effects.

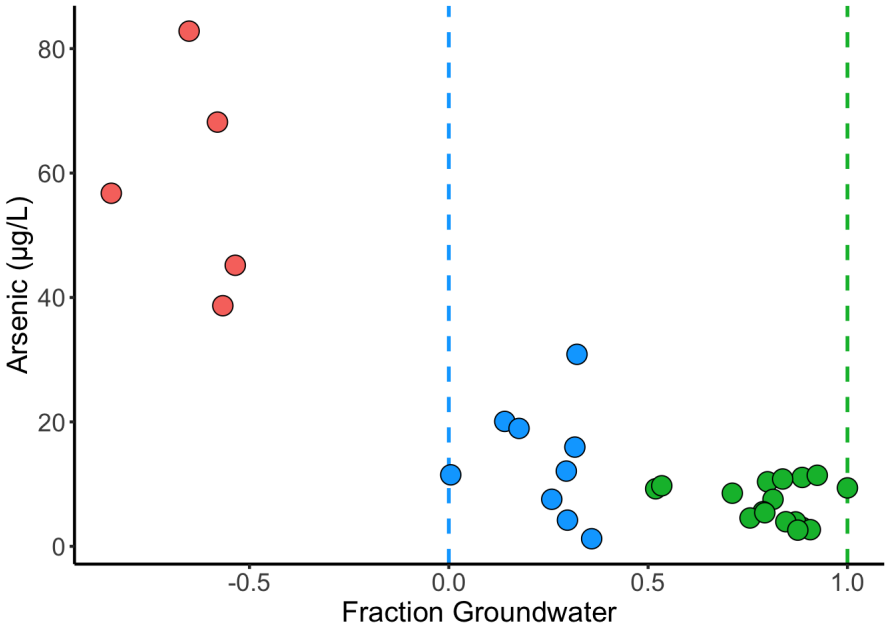

Figure 3.5: Streamwater samples percent groundwater vs. Arsenic for summer samples grouped by water source composition (eg. Groundwater vs precipitation). Blue line shows 100% precipitation, green line shows 100% groundwater with adjusted value. Blue points show precicipitation dominance, green points show groundwater dominance, red points show samples that fall outside the mixing model.

Winter

Compared to summer samples, winter samples are harder to explain. The main difference between the two seasons is a vastly lower $\delta^{18}O$ precipitation value. This means that $\delta^{18}O$ values being lower that the groundwater end member (green line) now show groundwater dominant source which is the inverse of what we saw in the summer. As seen in Figure 3.6, all but 2 of the points are more than 100% groundwater and fall in the the error category (red and purple). The only points that don't are two points (green) that appear to be groundwater dominant. Similarly to summer however, the red points may be explainable by evaporation. As seen in Figure 3.6 and 3.7 the red points again have lower d-excess values and higher arsenic values. They are both proportionally lower than summer samples but this is straightforward as more evaporation occurs during the warmer summer season.

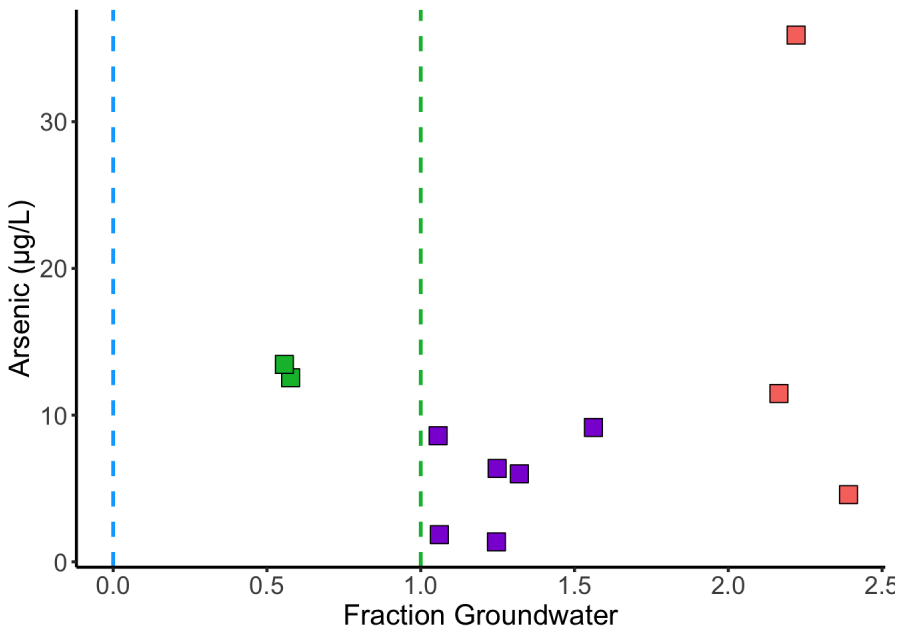

Figure 3.6: Streamwater samples percent groundwater vs. Arsenic for winter samples grouped by water source composition (eg. Groundwater vs precipitation). Blue line shows 100% precipitation, green line shows 100% groundwater. Blue points show precicipitation dominance, green points show groundwater dominance, purple and red points show samples that fall outside the mixing model.

In an attempt to better understand winter samples I added the summer groundwater sample as an end member in Figure 3.7. As we can see this causes all points to fall on the right side of the line with none present near precipitation. Compared to the summer graph it looks very different. Despite this, if we account for the cold winter climate in South Dakota it appears more reasonable. Since the vast majority of precipitation in the winter comes in the form of snow along side constant cold temperatures there may be little to no precipitation runoff in the region at the time. This means that our samples are likely entirely from groundwater recharge.

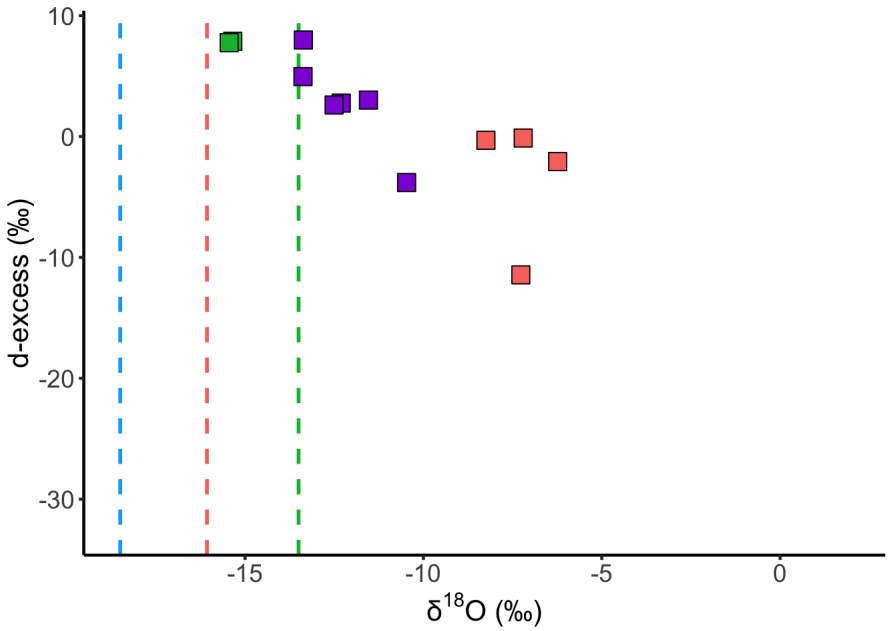

Figure 3.7: D-excess vs. $\delta^{18}O$ grouped for winter samples by water source composition (eg. Groundwater vs precipitation). Blue line shows precipitation endmenber, green line shows groundwater endmember, and red line shows new groundwater endmember. Blue points show precicipitation dominance, green points show groundwater dominance, purple and red points show possible errors.

Hydrograph

When comparing both summer (July and August) and winter (December) samples they both share the same relationship between d-excess and $\delta^{18}O$ (Figure 3.4 and 3.7). The only difference is the range in which values extend. This difference is likely due to the prevalence of warmer conditions in the summer enabling increased evaporation and more depleted d-excess values. Based on the claims that the winter samples were almost completely consistent of groundwater and the fact that both sample times share the same trend, it is possible that the summer samples are also consist primarily of groundwater.

To attempt to generally understand the composition of baseflow the use of a hydrograph can be helpful. A hydrograph is a way to display stream water level over time and allows for the impacts of storms on water level to be seen (*Hydrology Education: Hydrographs*, n.d.). Since quick flow (precipitation runoff) and baseflow travel at different speeds it is easy to see where the two sources are presumed to be dominant. On a hydrograph there are three primary trends visible. First is a large spike up which generally indicates a storm where much of the height increase is due to the rapid overland travel of quick flow. The magnitude of the spike also generally indicate storm size as larger storms tend to produce larger water height increases. The second is residual baseflow after a storm due some of the water infiltrating the ground. This is seen as a more gradual curve downward after the initial spike. The time between the peak and the end of the curve can indicate the residence time of water with more gradual curves showing longer times. The last trend is groundwater baseflow. This can usually be seen where the line remains flat as no new sources are causing variations.

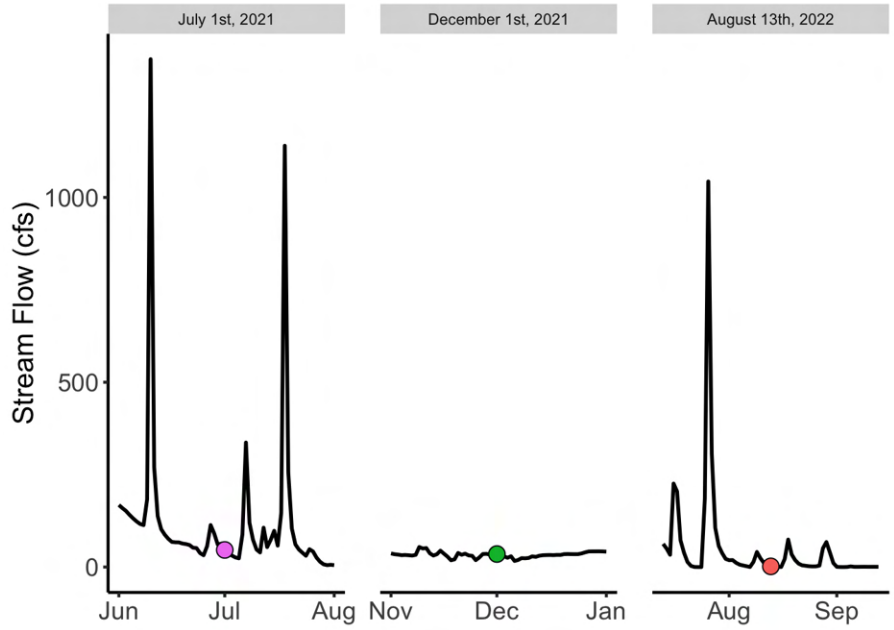

Figure 3.8: Hydrograph of each sample time from 6446500 (n.d.). Pink shows July 1st 2021, green shows December 1st 2021, and red shows August 13th 2022. Black lines shows the average dailey discharge (cfs) from each day. The lines span 1 month before and after each sample date. Gaps in December data likely due to the presence of ice.

Since my samples only account for a single point in time I created a hydrograph using a USGS stream site located on the white river in the northern center of the study area (6446500, n.d.). While this is not able to show accurate stream heights for each site it will allow us to generally see the impacts of quick flow and baseflow in the region. The first feature recognizable on the hydrograph is the stark difference between the summer (July and August) and winter (December) sampling dates (Figure 3.8). The winter date shows that there is little to no variation in the stream height leading up to the sampling date. This could imply that there has been very little precipitation and groundwater baseflow is the main source of water input. The summer sampling dates on the other hand have very noticeable storm inputs before and after each date which holds true in all late spring and summertime months (Figure 3.8 and 2.2). One feature visible in the hydrograph is the very short residence times of most storms. After each peak water height decreases to its original level not long after the storm. Both of our summer samples come right at the end of one of these peaks which means that they likely have a minimal amount of precipitation through both quick flow and baseflow left in their composition. This means that the majority of the water in our samples is likely from groundwater baseflow mixed with minimal amounts of precipitation.

Water Lines

If a groundwater is the dominant source of water in the streams in our study area then it can be hypothesized that evaporation seen through d-excess is the main cause of $\delta^{18}O$ enrichment. We can back up this claim by plotting each monthly average precipitation end member to find the Local Meteoric Water Line (LMWL). We found that LMWL had a slope of 7.768 which is very similar to the GMWL slope of 8 from Equation (2.3) (Figure (**ref?**)(fig:allwl)). Comparing both of these to our LSWL slope of 5.986 (Equation (2.4)) we can see that the variation is not due to the source but rather due to the local environment. We can also see our average predicted groundwater end member with a slope of 3.01 but as previously discussed the likely groundwater end-member is closer to -16‰ rather than -13.5‰.

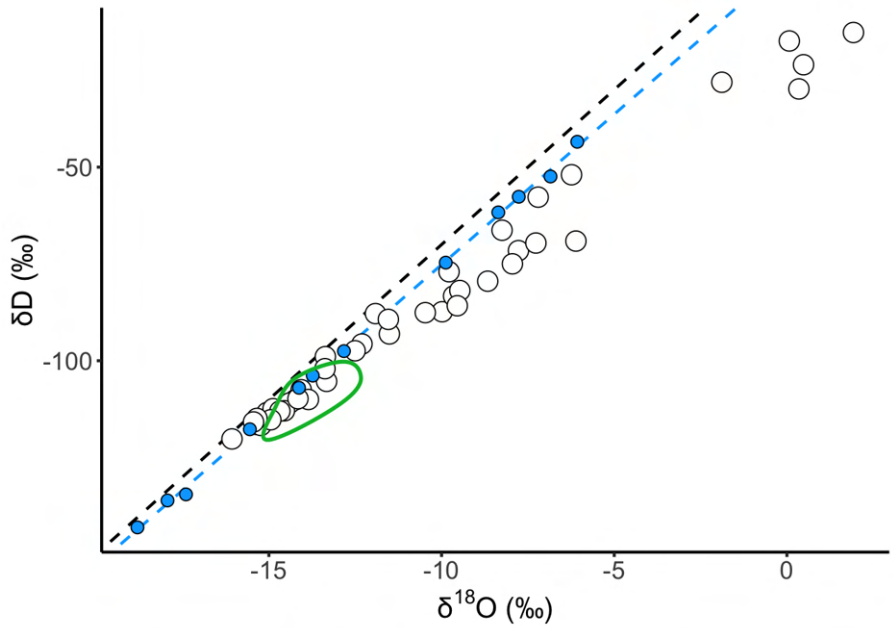

Figure 3.9: Relationship between δD and $\delta^{18}O$. Black line shows GMWL. White points show our study samples. Blue points show predicted monthly precipitation isotopes (Obtained from Bowen (2023)). Blue line represents the LMWL. Green elipse represents the range of predicted groundwater values (Obtained from M. O. Stahl, Gehring, and Jameel (2020))

Line-Conditioned Excess

One way to tease out ways water may differs from its source is by using line-conditioned excess (lc-excess). Lc-excess is defined as:

\begin{equation} \text{lc-excess} = δD - A \timesδ^{18}O - B \tag{3.4} \end{equation}

where A is the slope of my LSWL (Equation (2.4)) and B is the intercept (Landwehr, Jurate Maciunas and Coplen, Tyler B. 2004). The slope for our equation was 5.986 and the intercept was -23.722 (Equation (2.3)). As seen in Figure 3.10, samples are now broken in to two groups. According to Landwehr, Jurate Maciunas and Coplen, Tyler B. (2004), samples above the line (blue/purple) suggest moisture source differences and points below the line (orange/yellow) are indicative of evaporation. However, due to the use of my LSWL instead of my LMWL the points above (blue/purples) and points below (orange/yellow) instead show two possible different moisture sources (Figure 3.10).

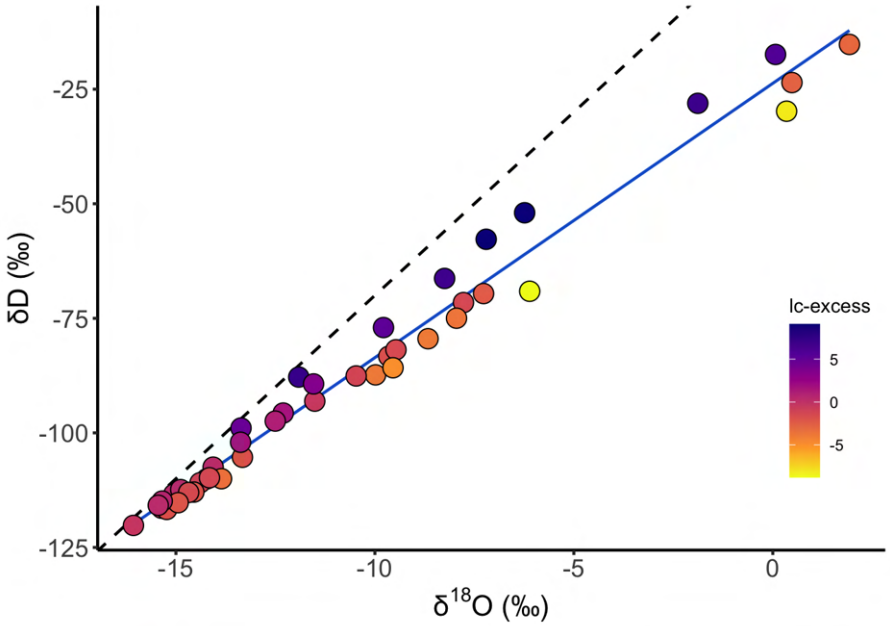

Figure 3.10: Scatter plot between $\delta^{18}O$ and δD colored by lc-excess. Local Stream Water Line in blue. Global Meteoric Water Line in black.

By grouping point on either side of the line together (Figure 3.11 we can get a better understanding of why they vary. The samples below the LSWL (green) likely show the normal local source of water. The samples above the LSWL (blue) implies the presence of a secondary water source. The slopes of the groups also change from the original 5.986 where the upper group (blue) now has a slope of 6.502 and the lower group now has a slope of 5.747 (Figure 3.11). One possible cause of the second source is the seasonality in our samples. A large proportion of the winter samples fall within the group above the LMWL (blue squares). By comparing each samples season and lc-excess in a t-test I found that it had a p-value of 0.004437 meaning the relationship between season was significant. This means that being above the line (blue) shows a winter origin and being below (green) the line shows summer origin (Figure 3.11). While this is predominantly true there is a few outliers for both summer and winter samples. One possible explanation for this the presence of some precipitation water in the samples. This would cause the pre-evaporation isotopes of the upper lc-excess samples to have a different isotopic identity than the other samples causing the alternative slope.

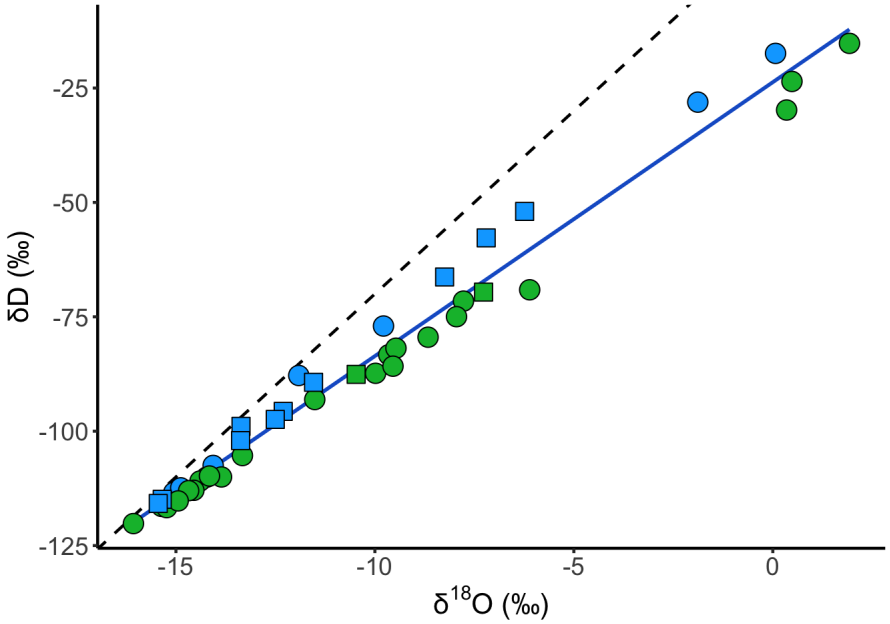

Figure 3.11: Scatter plot between $\delta^{18}O$ and δD colored by lc-excess groupings. Global Meteoric Water Line in black. Local Surface Water Line in blue. Squares shows winter samples and circles show summer samples.

Cause Combination

To better understand the affects of each environmental affect on the arsenic concentration in the region we can combine our lc-excess (Figure 3.11), and the d-excess groups (Figure 2.28). This leaves us with 5 different grouping. Like in Figure 3.11 the green points follow the lower lc-excess trend (mostly summer) and the blue points follow the upper lc-excess trend (mostly winter). The pink error points also fit the mostly winter trend well but will remain separated. We can also see the high d-excess group being the lighter colors and the low d-excess group being darker colors (Figure 2.28).

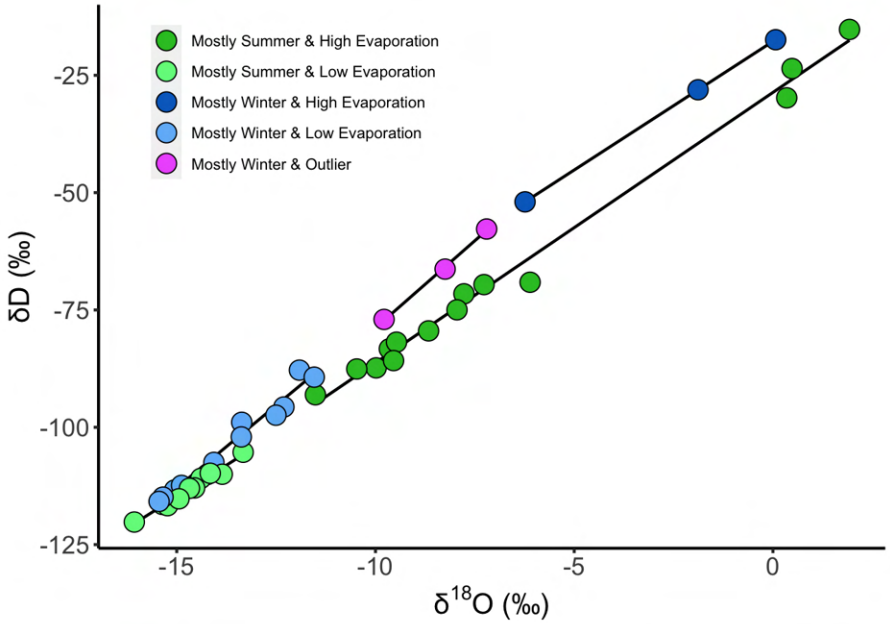

Figure 3.12: Scatter plot between $\delta^{18}O$ and δD colored by joint lc-excess and d-excess groupings. Black lines show trend of each group. See legend for colors.

By adding our color grouping to our $\delta^{18}O$ vs Arsenic figure (2.28 we can see some distinct trends emerging (Figure 3.13). The first trend is the similarity between both low evaporation samples despite having predominantly different seasonal sources. This further shows the impact of evaporation on changing the isotopic composition of the water. Additionally between these two groups we can also see the source difference indicative of each season. For the high evaporation groups we can see that they both increase in arsenic as $\delta^{18}O$ increases however it appears as they have different trend lines.

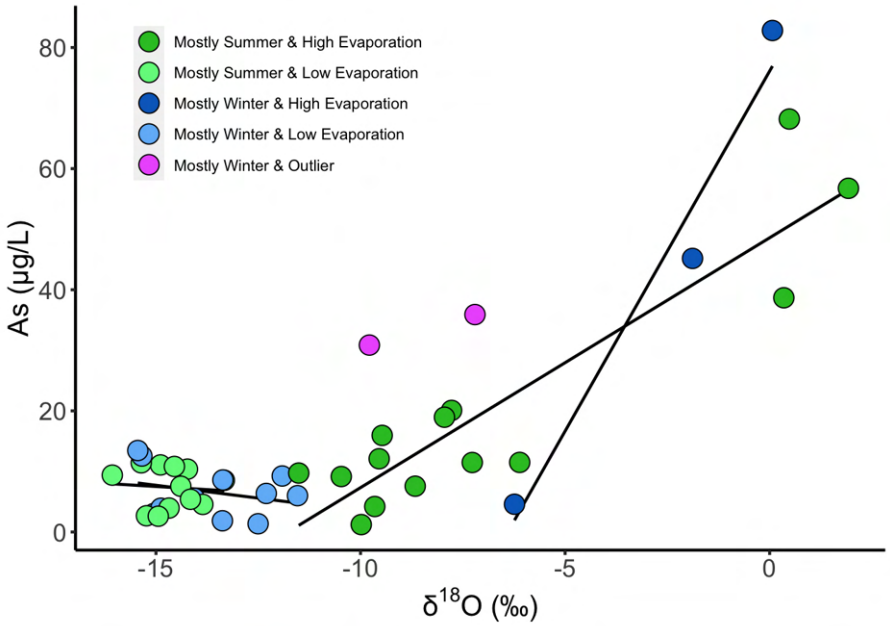

Figure 3.13: Scatter plot between $\delta^{18}O$ and Arsenic colored by joint lc-excess and d-excess groupings. Black lines show trend of each group. See legend for colors.

While Figure 3.13 shows distinct trends it doesn't account well for the pink error points or the samples with some precipitation in Figure 3.11. To account for each of these options I created a flow chart breaking each sample in to a distinct group. The groups break the sample in to season, lc-excess groups, d-excess groups, arsenic groups and by notable surface geology. This resulted in six groups with notable variation and three groups with regular variation. The regular variation groups ('many' in the figure) show samples with a groundwater source and isotope enrichment primarily due to evaporation.

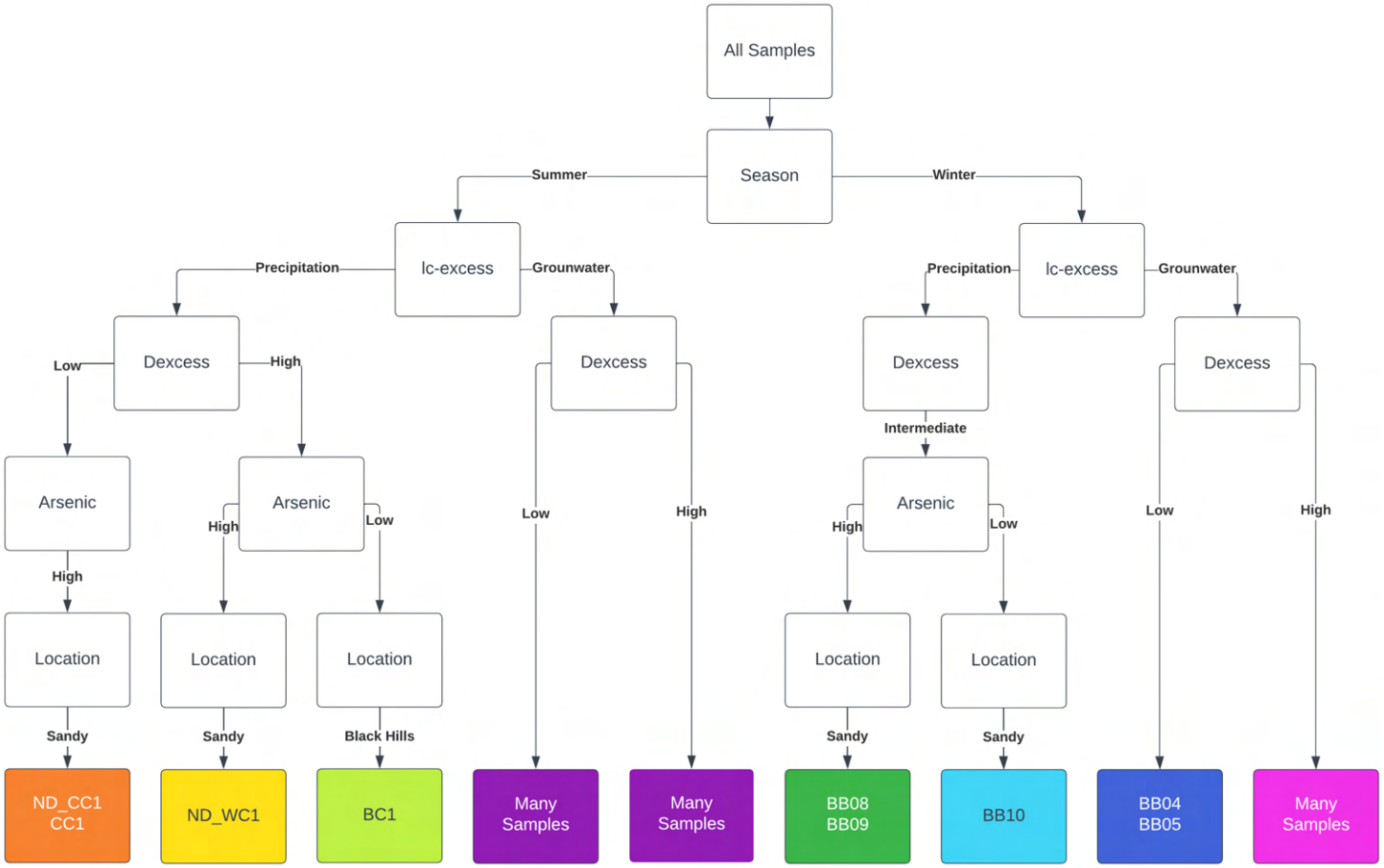

Figure 3.14: Flow chart showing the posible variation for the samples. Bottom row shows variation groups. Bubbles with 'Many' indicate many samples that are explaied by expected groundwater source and d-excess evaporation.

Summer and Winter variation

By grouping the samples using the flowchart (Figure 3.14) we can now explain each source of variation in our region (Figure 3.15). Starting with summer we first see the largest group of samples (purple). This group can be classified as our expected summer water line. This grouping consists of primarily groundwater samples as concluded by our mixing model and our lc-excess grouping (Figure 3.11). The remaining summer samples (light green, yellow, and orange) all fall off this expected trend. The main reason for this is the difference in lc-excess as they fall in the 'mostly winter' group despite being summer samples (Figure 3.11). This suggests an alternative source of water which in this case is likely the presence of some precipitation in the sample. Looking closer at the ND_WC1 sample (yellow) and the CC1 samples (orange), we can see they have abnormally high arsenic values comparatively to the purple samples with the same d-excess. If the alternative source of water is due to added precipitation we can predict that the elevated arsenic is in some way caused by this precipitation. Finding these three samples (ND_WC1, ND_CC1, and CC1) on a map we can see that they all are in close proximity to the sandy terrain of the Badlands (Figure 2.1) and Toadstool Geological park (Figure 3.16). This would suggest that a recent storm caused elevated levels of arsenic likely by washing away sediment into the stream. To confirm that the alternative source is likely precipitation we can look closer at BC1 (light green). This sample falls farthest outside the main study area in the Black Hills (Figure 3.16). This means that it likely contains more precipitation from increased precipitation falling in the higher elevation mountains.

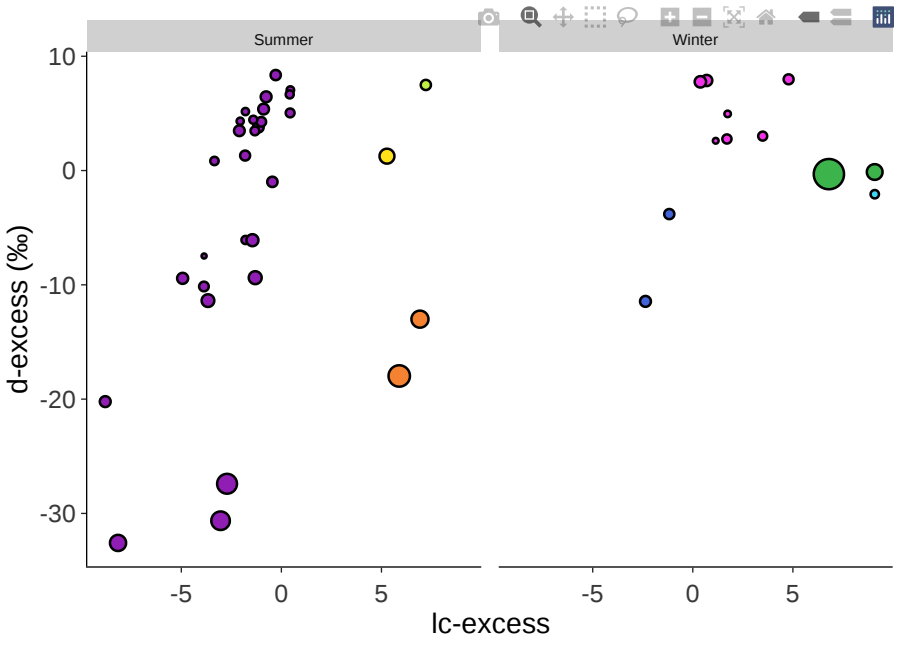

Figure 3.15: Scatter plot based on flow chart for summer and winter samples. Groups created from d-excess, lcexcess, season and other variables. Groups explained in text. Hover with mouse to see more info on each point.

Moving on to the winter samples we see some similar patters compared to the summer samples. The first similarity is between the pink and dark blue samples. They share a similar pattern to the main summer trend (purple) and can be can also be considered the main winter group. The reason the dark blue points are colored separately is they fell in to the mostly summer lc-excess group (Figure 3.11) despite being winter points. Rather than being the result of precipitation like the summer samples that crossed the lc-excess line, these two samples were likely follow the regular winter line as there was minimal precipitation in the winter (Figure 3.8). The remaining two green points and one light blue point are very similar but have very different arsenic concentration. The green points were already discussed as being within the sandy Badlands Region. However, the blue sample, located right next to these samples (Figure 3.16), has a much lower amount of arsenic. One possible reason is where each of these points was collected. Looking at the map (Figure 3.16), these three samples may have all been collected from small pools of water or small dams. This could have caused enrichment of arsenic in pool where runoff from the sandy sediment could reach and simultaneously prevent arsenic sediment from reaching another. This could also prevent the inflow of groundwater if a confining layer is in place resulting in the water being more consistent of precipitation in comparison. More study in to these three sample sites would be needed to fully understand if these prediction are true.

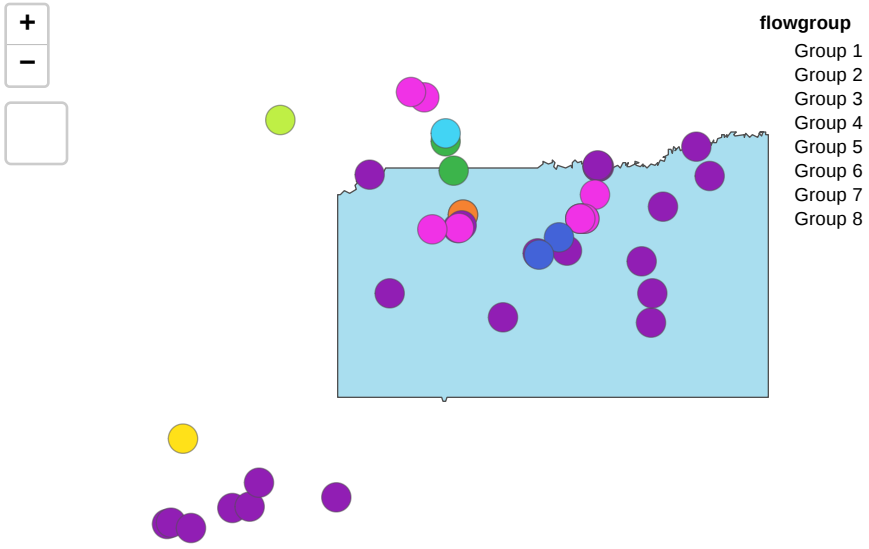

Figure 3.16: Map of samples colored by flow chart groupings. Colors cordinate to the figure above.

4 Conclusion

The primary aim of this study was to leverage the spatial data to understand the mobilization mechanisms of As and U into drinking water in the Northern Plains. Based on our finding we can make numerous distinct conclusions. First is that almost all samples had elevated amounts of arsenic and uranium near or above the EPA guidelines. This is a concern on a basic level as it implies that almost all of the water in the Pine Ridge Reservation region. In the study area overall the primary method for arsenic and uranium enrichment above base levels due to excess evaporation in the warm summer months, specifically August. This enrichment comes from groundwater with moderate levels that doubles and triples in concentration due to the extreme evaporative conditions. The secondary pathway for enrichment is precipitation runoff collecting arsenic and uranium rich sediment from region like the Bad Lands. These pathways combined create dangerous levels of contamination in some regions and should be avoided is able. Some future research the better analyse the contamination in the Pine Ridge Reservation would be looking in depth in to groundwater samples. This would allow us to understand on an individual level if arsenic and uranium concentrations were caused by high levels in the pre-existing sediment or if the evaporative enrichment is a cause of well contamination. Overall arsenic and uranium are both hazardous metals and continued research in to the topic specifically in the Pine Ridge Reservation is crucial for the continued safety of the local community.

Acknowledgements

I would like to acknowledge and give thanks to my supervisor Mason Stahl who made this work possible and Benjamin Bostick for his support, mentorship, and scientific contributions throughout this project. Their guidance and interest in my research enabled me to fully develop my thesis. I would also like to give thanks to my parents and girlfriend for their continuous support. Lastly, special thanks to my thesis lab partners Christine Swanson and Grace Levins as well as the other members of the map room for supporting my work. This research was supported by a grant from the NIH Superfund Research Program (P42ES033719) and an NSF MRI grant (2018836).

References

1 in 3 People Globally Do Not Have Access to Safe Drinking Water – UNICEF, WHO. 2019. World Health Organization. https://www.who.int/news/item/18-06-2019-1-in-3-people-globally-do-not-have-access-to-safe-drinking-water-unicef-who (https://www.who.int/news/item/18-06-2019-1-in-3-people-globally-do-not-have-access-to-safe-drinking-water-unicef-who).

6446500. n.d. *WHITE R NEAR INTERIOR,SD*. United States Geological Survey. https://waterdata.usgs.gov/monitoring-location/06446500/#parameterCode=00065&period=P7D (https://waterdata.usgs.gov/monitoring-location/06446500/#parameterCode=00065&period=P7D).

Affolter, Stéphane, Anamaria D. Häuselmann, Dominik Fleitmann, Philipp Häuselmann, and Markus Leuenberger. 2015. "Triple Isotope (δD, δ17O, δ18O) Study on Precipitation, Drip Water and Speleothem Fluid Inclusions for a Western Central European Cave (NW Switzerland)." *Quaternary Science Reviews* 127 (November): 73–89. https://doi.org/10.1016/j.quascirev.2015.08.030 (https://doi.org/10.1016/j.quascirev.2015.08.030).

Alam, Md. Samrat, and Tao Cheng. 2014. "Uranium Release from Sediment to Groundwater: Influence of Water Chemistry and Insights into Release Mechanisms." *Journal of Contaminant Hydrology* 164 (August): 72–87. https://doi.org/10.1016/j.jconhyd.2014.06.001 (https://doi.org/10.1016/j.jconhyd.2014.06.001).

American Community Survey 5-Year Estimates. 2021. U.S. Census Bureau. https://censusreporter.org/profiles/25000US2810-pine-ridge-reservation/ (https://censusreporter.org/profiles/25000US2810-pine-ridge-reservation/).

Arsenic. 2021. Environmental Working Group. https://www.ewg.org/tapwater/reviewed-arsenic.php (https://www.ewg.org/tapwater/reviewed-arsenic.php).

———. 2022. World Health Organization. https://www.who.int/news-room/fact-sheets/detail/arsenic (https://www.who.int/news-room/fact-sheets/detail/arsenic).

Arsenic Factsheet. 2017. Centers for Disease Control; Prevention. https://www.cdc.gov/biomonitoring/Arsenic_FactSheet.html (https://www.cdc.gov/biomonitoring/Arsenic_FactSheet.html).

Ashbolt, Nicholas John. 2004. "Microbial Contamination of Drinking Water and Disease Outcomes in Developing Regions." *Toxicology* 198 (1-3): 229–38. https://doi.org/10.1016/j.tox.2004.01.030 (https://doi.org/10.1016/j.tox.2004.01.030).

Azizur Rahman, M., H. Hasegawa, M. Mahfuzur Rahman, M. A. Mazid Miah, and A. Tasmin. 2008. "Arsenic Accumulation in Rice (Oryza Sativa L.): Human Exposure Through Food Chain." *Ecotoxicology and Environmental Safety* 69 (2): 317–24. https://doi.org/10.1016/j.ecoenv.2007.01.005 (https://doi.org/10.1016/j.ecoenv.2007.01.005).

Balazs, Carolina L, Rachel Morello-Frosch, Alan E Hubbard, and Isha Ray. 2012. "Environmental Justice Implications of Arsenic Contamination in California's San Joaquin Valley: A Cross-Sectional, Cluster-Design Examining Exposure and Compliance in Community Drinking Water Systems." *Environmental Health* 11 (1). https://doi.org/10.1186/1476-069x-11-84 (https://doi.org/10.1186/1476-069x-11-84).

Bershaw, John. 2018. "Controls on Deuterium Excess Across Asia." *Geosciences* 8 (7): 257. https://doi.org/10.3390/geosciences8070257 (https://doi.org/10.3390/geosciences8070257).

Bershaw, John, Dougal D. Hansen, and Andrew J. Schauer. 2020. "Deuterium Excess and ¹⁷o-Excess Variability in Meteoric Water Across the Pacific Northwest, USA." *Tellus B: Chemical and Physical Meteorology* 72 (1): 1773722. https://doi.org/10.1080/16000889.2020.1773722 (https://doi.org/10.1080/16000889.2020.1773722).

Bondy, Stephen, and Arezoo Campbell. 2017. "Water Quality and Brain Function." *International Journal of Environmental Research and Public Health* 15 (1): 2. https://doi.org/10.3390/ijerph15010002 (https://doi.org/10.3390/ijerph15010002).

Bowen, Gabe. 2023. *Waterisotopes Database*. University of Utah. http://waterisotopes.org (http://waterisotopes.org).

Carter, Janet M., and Allen J. Heakin. 2007. "Generalized Potentiometric Surface of the Arikaree Aquifer, Pine Ridge Indian Reservation and Bennett County, South Dakota." *Scientific Investigations Map*. https://doi.org/10.3133/sim2993 (https://doi.org/10.3133/sim2993).

Chemical Contaminant Rules. 2022. United States Environmental Protection Agency. https://www.epa.gov/dwreginfo/chemical-contaminant-rules (https://www.epa.gov/dwreginfo/chemical-contaminant-rules).

Communications, and Publishing. 2015. *About 115 Million People—More Than One-Third of the Nation's Population—Rely on Groundwater for Drinking Water. As the Nation's Population Grows, the Need for High-Quality Drinking-Water Supplies Becomes Even More Urgent.* United States Geological Survey. https://www.usgs.gov/news/featured-story/quality-nations-groundwater (https://www.usgs.gov/news/featured-story/quality-nations-groundwater).

Craig, Harmon. 1961. "Isotopic Variations in Meteoric Waters." *Science* 133 (3465): 1702–3. https://doi.org/10.1126/science.133.3465.1702 (https://doi.org/10.1126/science.133.3465.1702).

Dansgaard, W. 2012. "Stable Isotopes in Precipitation." *Tellus A: Dynamic Meteorology and Oceanography* 16 (4): 436. https://doi.org/10.3402/tellusa.v16i4.8993 (https://doi.org/10.3402/tellusa.v16i4.8993).

Delpla, I., A.-V. Jung, E. Baures, M. Clement, and O. Thomas. 2009. "Impacts of Climate Change on Surface Water Quality in Relation to Drinking Water Production." *Environment International* 35 (8): 1225–33. https://doi.org/10.1016/j.envint.2009.07.001 (https://doi.org/10.1016/j.envint.2009.07.001).

Division, Public Health. 2021. *Arsenic and Drinkingwater*. Oregon Health Advisory. https://www.oregon.gov/oha/ph/healthyenvironments/drinkingwater/monitoring/documents/health/arsenic.pdf (https://www.oregon.gov/oha/ph/healthyenvironments/drinkingwater/monitoring/documents/health/arsenic.pdf).

Fendorf, Scott, Holly A. Michael, and Alexander van Geen. 2010. "Spatial and Temporal Variations of Groundwater Arsenic in South and Southeast Asia." *Science* 328 (5982): 1123–27. https://doi.org/10.1126/science.1172974 (https://doi.org/10.1126/science.1172974).

Freeze, R. Allan. 1974. "Streamflow Generation." *Reviews of Geophysics* 12 (4): 627. https://doi.org/10.1029/rg012i004p00627 (https://doi.org/10.1029/rg012i004p00627).

Friedman, Irving, Alfred C. Redfield, Beatrice Schoen, and Joseph Harris. 1964. "The Variation of the Deuterium Content of Natural Waters in the Hydrologic Cycle." *Reviews of Geophysics* 2 (1): 177. https://doi.org/10.1029/rg002i001p00177 (https://doi.org/10.1029/rg002i001p00177).

Fry, Brian. 2006. *Stable Isotope Ecology*. Springer New York. https://doi.org/10.1007/0-387-33745-8 (https://doi.org/10.1007/0-387-33745-8).

Geen, Alexander van, Benjamín C. Bostick, Pham Thi Kim Trang, Vi Mai Lan, Nguyen-Ngoc Mai, Phu Dao Manh, Pham Hung Viet, et al. 2013. "Retardation of Arsenic Transport Through a Pleistocene Aquifer." *Nature* 501 (7466): 204–7. https://doi.org/10.1038/nature12444 (https://doi.org/10.1038/nature12444).

Geishirt Cantrell, Betty A., Felicia Hodge, Roxanne Struthers, and Lorelei Decora. 2005. "The High Incidence of Cigarette Smoking Among American Indians of the Northern Plains." *Journal of Cancer Education* 20 (March): 97–100. https://doi.org/10.1207/s15430154jce2001s_19 (https://doi.org/10.1207/s15430154jce2001s_19).

Geologic Activity. 2020. National Park Service. https://www.nps.gov/articles/000/badl-geologic-formations.htm (https://www.nps.gov/articles/000/badl-geologic-formations.htm).

Geologic Formations: How Badlands Buttes Came to Be. 2020. National Park Service. https://www.nps.gov/articles/000/badl-geologic-formations.htm (https://www.nps.gov/articles/000/badl-geologic-formations.htm).

Global Issues. n.d. United Nations. https://www.un.org/en/global-issues (https://www.un.org/en/global-issues).

Gonzales, A. L., J. Nonner, J. Heijkers, and S. Uhlenbrook. 2009. "Comparison of Different Base Flow Separation Methods in a Lowland Catchment." *Hydrology and Earth System Sciences* 13 (11): 2055–68. https://doi.org/10.5194/hess-13-2055-2009 (https://doi.org/10.5194/hess-13-2055-2009).

"Ground Water Atlas of the United States: Segment 8, Montana, North Dakota, South Dakota, Wyoming." 1996. https://doi.org/10.3133/ha730i (https://doi.org/10.3133/ha730i).

Hackley, Randall. 2018. *The World's Natural Aquifers at Risk*. Stockholm International Water Institute. https://siwi.org/latest/the-worlds-natural-aquifers-at-risk/#:~:text=Increasing%20populations%2C%20including%20those%20migrating,their%20primary%20source%20of%20water (https://siwi.org/latest/the-worlds-natural-aquifers-at-risk/#:~:text=Increasing%20populations%2C%20including%20those%20migrating,their%20primary%20source%20of%20water).

Herath, Indika, Meththika Vithanage, Jochen Bundschuh, Jyoti Prakash Maity, and Prosun Bhattacharya. 2016. "Natural Arsenic in Global Groundwaters: Distribution and Geochemical Triggers for Mobilization." *Current Pollution Reports* 2 (1): 68–89. https://doi.org/10.1007/s40726-016-0028-2 (https://doi.org/10.1007/s40726-016-0028-2).

Hydrology Education: Hydrographs. n.d. National Weather Service. https://www.weather.gov/lot/hydrology_education_hydrographs (https://www.weather.gov/lot/hydrology_education_hydrographs).

Jung, Hyejung, Dong-Chan Koh, Yun Kim, Sung-Wook Jeen, and Jeonghoon Lee. 2020. "Stable Isotopes of Water and Nitrate for the Identification of Groundwater Flowpaths: A Review." *Water* 12 (1): 138. https://doi.org/10.3390/w12010138 (https://doi.org/10.3390/w12010138).

Kalbus, E., F. Reinstorf, and M. Schirmer. 2006. "Measuring Methods for Groundwater Surface Water Interactions: A Review." *Hydrology and Earth System Sciences* 10 (6): 873–87. https://doi.org/10.5194/hess-10-873-2006 (https://doi.org/10.5194/hess-10-873-2006).

Konikow, Leonard F., and Eloise Kendy. 2005. "Groundwater Depletion: A Global Problem." *Hydrogeology Journal* 13 (1): 317–20. https://doi.org/10.1007/s10040-004-0411-8 (https://doi.org/10.1007/s10040-004-0411-8).

Lall, Upmanu, Laureline Josset, and Tess Russo. 2020. "A Snapshot of the World's Groundwater Challenges." *Annual Review of Environment and Resources* 45 (1): 171–94. https://doi.org/10.1146/annurev-environ-102017-025800 (https://doi.org/10.1146/annurev-environ-102017-025800).

Landwehr, Jurate Maciunas and Coplen, Tyler B. 2004. *R: Line-Conditioned Excess: A New Method for Characterizing Stable Hydrogen and Oxygen Isotope Ratios in Hydrologic Systems*. *International Conference on Isotopes in Environmental*.

Leading Causes of Death. 2023. Centers for Disease Control; Prevention. https://www.cdc.gov/nchs/fastats/leading-causes-of-death.htm (https://www.cdc.gov/nchs/fastats/leading-causes-of-death.htm).

Leonard, Ciara. 2021. *Indigenous Tribe Battle Crow Butte Uranium Mine, Nebraska, USA*. Environmental Justice Atlas. https://ejatlas.org/conflict/indigenous-tribes-battle-crow-butte-uranium-mine-nebraska-usa (https://ejatlas.org/conflict/indigenous-tribes-battle-crow-butte-uranium-mine-nebraska-usa).

Marshall, John D., J. Renee Brooks, and Kate Lajtha. n.d. "Sources of Variation in the Stable Isotopic Composition of Plants." In, 22–60. Blackwell Publishing Ltd. https://doi.org/10.1002/9780470691854.ch2 (https://doi.org/10.1002/9780470691854.ch2).

Martin, J. E., J. F. Sawyer, M. D. Fahrenbach, D. W. Tomhave, and L. D. Schulz. 2004. *Geologic Map of South Dakota*. South Dakota Geological Survey. https://ngmdb.usgs.gov/Prodesc/proddesc_72317.htm (https://ngmdb.usgs.gov/Prodesc/proddesc_72317.htm).

Medzerian, Paul, Jeff Newman, and Connie O'Connell. 2022. *Personal Income by County and Metropolitan Area, 2021*. The Bureau of Economic Analysis. https://www.bea.gov/sites/default/files/2022-11/lapi1122.pdf (https://www.bea.gov/sites/default/files/2022-11/lapi1122.pdf).

Mondal, Debapriya, and David A. Polya. 2008. "Rice Is a Major Exposure Route for Arsenic in Chakdaha Block, Nadia District, West Bengal, India: A Probabilistic Risk Assessment." *Applied Geochemistry* 23 (11): 2987–98. https://doi.org/10.1016/j.apgeochem.2008.06.025 (https://doi.org/10.1016/j.apgeochem.2008.06.025).

Monthly National Climate Report for Annual 2020. 2021. NOAA National Centers for Environmental Information. https://www.ncei.noaa.gov/access/monitoring/monthly-report/national/202013 (https://www.ncei.noaa.gov/access/monitoring/monthly-report/national/202013).

National App. n.d. United States Geological Survey. https://apps.nationalmap.gov/viewer/ (https://apps.nationalmap.gov/viewer/).

Nghiem, Athena A., Mason O. Stahl, Brian J. Mailloux, Tran Thi Mai, Pham Thi Trang, Pham Hung Viet, Charles F. Harvey, Alexander Geen, and Benjamin C. Bostick. 2019. "Quantifying Riverine Recharge Impacts on Redox Conditions and Arsenic Release in Groundwater Aquifers Along the Red River, Vietnam." *Water Resources Research* 55 (8): 6712–28. https://doi.org/10.1029/2019wr024816 (https://doi.org/10.1029/2019wr024816).

Oglala Lakota County, South Dakota Precipitation. n.d. NOAA National Centers for Environmental Information. https://www.ncei.noaa.gov/access/monitoring/climate-at-a-glance/county/time-series/SD-102/pcp/ann/1/1895-2023 (https://www.ncei.noaa.gov/access/monitoring/climate-at-a-glance/county/time-series/SD-102/pcp/ann/1/1895-2023).

Phillips, Donald L., Seth D. Newsome, and Jillian W. Gregg. 2005. "Combining Sources in Stable Isotope Mixing Models: Alternative Methods." *Oecologia* 144 (4): 520–27. https://doi.org/10.1007/s00442-004-1816-8 (https://doi.org/10.1007/s00442-004-1816-8).

Ravalli, Filippo, Yuanzhi Yu, Benjamin C Bostick, Steven N Chillrud, Kathrin Schilling, Anirban Basu, Ana Navas-Acien, and Anne E Nigra. 2022. "Sociodemographic Inequalities in Uranium and Other Metals in Community Water Systems Across the USA, 200611: A Cross-Sectional Study." *The Lancet Planetary Health* 6 (4): e320–30. https://doi.org/10.1016/s2542-5196(22)00043-2 (https://doi.org/10.1016/s2542-5196(22)00043-2).

Resources, Water. 2019a. *Oxidation/Reduction (Redox)*. United States Geological Survey. https://www.usgs.gov/mission-areas/water-resources/science/oxidationreduction-redox (https://www.usgs.gov/mission-areas/water-resources/science/oxidationreduction-redox).

———. 2019b. *Domestic (Private) Supply Wells*. United States Geological Survey. https://www.usgs.gov/mission-areas/water-resources/science/domestic-private-supply-wells (https://www.usgs.gov/mission-areas/water-resources/science/domestic-private-supply-wells).

———. 2019c. *Arsenic and Drinking Water*. United States Geological Survey. https://www.usgs.gov/mission-areas/water-resources/science/arsenic-and-drinking-water (https://www.usgs.gov/mission-areas/water-resources/science/arsenic-and-drinking-water).

Shaw, W. Douglass, Mark Walker, and Marnee Benson. 2005. "Treating and Drinking Well Water in the Presence of Health Risks from Arsenic Contamination: Results from a U.S. Hot Spot." *Risk Analysis* 25 (6): 1531–43. https://doi.org/10.1111/j.1539-6924.2005.00698.x (https://doi.org/10.1111/j.1539-6924.2005.00698.x).

Smedley, P. L, and D. G Kinniburgh. 2002. "A Review of the Source, Behaviour and Distribution of Arsenic in Natural Waters." *Applied Geochemistry* 17 (5): 517–68. https://doi.org/10.1016/s0883-2927(02)00018-5 (https://doi.org/10.1016/s0883-2927(02)00018-5).

Sobel, Marisa, Tiffany R. Sanchez, Tracy Zacher, Brian Mailloux, Martha Powers, Joseph Yracheta, David Harvey, et al. 2021. "Spatial Relationship Between Well Water Arsenic and Uranium in Northern Plains Native Lands." *Environmental Pollution* 287 (October): 117655. https://doi.org/10.1016/j.envpol.2021.117655 (https://doi.org/10.1016/j.envpol.2021.117655).

Stable Isotopes. n.d. International Atomic Energy Agency. https://www.iaea.org/topics/nuclear-science/isotopes/stable-isotopes (https://www.iaea.org/topics/nuclear-science/isotopes/stable-isotopes).

Stahl, Mason O., Jaclyn Gehring, and Yusuf Jameel. 2020. "Isotopic Variation in Groundwater Across the Conterminous United States Insight into Hydrologic Processes." *Hydrological Processes* 34 (16): 3506–23. https://doi.org/10.1002/hyp.13832 (https://doi.org/10.1002/hyp.13832).

Stahl, Mason, Jack Wassik, Jaclyn Gehring, Connor Horan, and Andrew Wozniak. 2021. "Connecting the Age and Reactivity of Organic Carbon to Watershed Geology and Land Use in Tributaries of the Hudson River." *Journal of Geophysical Research: Biogeosciences* 126 (9). https://doi.org/10.1029/2021jg006494 (https://doi.org/10.1029/2021jg006494).

Stolze, Lucien, Maria Battistel, and Massimo Rolle. 2022. "Oxidative Dissolution of Arsenic-Bearing Sulfide Minerals in Groundwater: Impact of Hydrochemical and Hydrodynamic Conditions on Arsenic Release and Surface Evolution." *Environmental Science & Technology* 56 (8): 5049–61. https://doi.org/10.1021/acs.est.2c00309 (https://doi.org/10.1021/acs.est.2c00309).

Sun, Jing, Andrew N. Quicksall, Steven N. Chillrud, Brian J. Mailloux, and Benjamin C. Bostick. 2016. "Arsenic Mobilization from Sediments in Microcosms Under Sulfate Reduction." *Chemosphere* 153 (June): 254–61. https://doi.org/10.1016/j.chemosphere.2016.02.117 (https://doi.org/10.1016/j.chemosphere.2016.02.117).

Tappa, Daniel J., Matthew J. Kohn, James P. McNamara, Shawn G. Benner, and Alejandro N. Flores. 2016. "Isotopic Composition of Precipitation in a Topographically Steep, Seasonally Snow-Dominated Watershed and Implications of Variations from the Global Meteoric Water Line." *Hydrological Processes* 30 (24): 4582–92. https://doi.org/10.1002/hyp.10940 (https://doi.org/10.1002/hyp.10940).

Technical Fact Sheet: Proposed Rule for Arsenic in Drinking Water and Clarifications to Compliance and New Source Contaminants Monitoring. 2000. United States Environmental Protection Agency. https://archive.epa.gov/water/archive/web/html/regulations_pro-techfactsheet.html (https://archive.epa.gov/water/archive/web/html/regulations_pro-techfactsheet.html).

The Role of Arsenic in the Mining Industry. 2015. Society for Mining, Metallurgy & Exploration. https://www.smenet.org/What-We-Do/Technical-Briefings/The-Role-of-Arsenic-in-the-Mining-Industry (https://www.smenet.org/What-We-Do/Technical-Briefings/The-Role-of-Arsenic-in-the-Mining-Industry).

"Toxicological Profile for Arsenic." 2007. https://doi.org/10.15620/cdc:11481 (https://doi.org/10.15620/cdc:11481).

"Toxicological Profile for Uranium." 2002. In. CRC Press. https://doi.org/10.1201/9781420061888_ch157 (https://doi.org/10.1201/9781420061888_ch157).

Vreča, Polona, and Zoltán Kern. 2020. "Use of Water Isotopes in Hydrological Processes." *Water* 12 (8): 2227. https://doi.org/10.3390/w12082227 (https://doi.org/10.3390/w12082227).

Water Contamination and Diseases. 2022. Centers for Disease Control; Prevention. https://www.cdc.gov/healthywater/drinking/contamination.html (https://www.cdc.gov/healthywater/drinking/contamination.html).

What Are the Routes of Exposure for Uranium? 2013. Centers for Disease Control; Prevention. https://www.atsdr.cdc.gov/csem/uranium/exposure_pathways.html (https://www.atsdr.cdc.gov/csem/uranium/exposure_pathways.html).

Yadav, Shailesh Kumar, A. L. Ramanathan, Manoj Kumar, S. Chidambaram, Y. P. Gautam, and C. Tiwari. 2020. "Assessment of Arsenic and Uranium Co-Occurrences in Groundwater of Central Gangetic Plain, Uttar Pradesh, India." *Environmental Earth Sciences* 79 (6). https://doi.org/10.1007/s12665-020-8892-x (https://doi.org/10.1007/s12665-020-8892-x).